

**DIGITAL IMAGE CORRELATION FOR
DEFORMATION MEASUREMENTS
NEAR A CRACK**

By

SAMPATHKUMAR PERIASAMY

Bachelor of Engineering

Government College of Technology

Coimbatore, India

1999

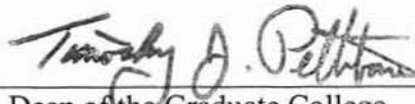
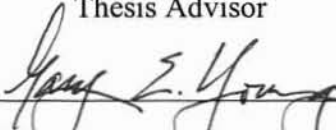
Submitted to the Faculty
of the Graduate College of
Oklahoma State University
in partial fulfillment of
the requirements for
the Degree of
MASTER OF SCIENCE
December, 2002

**DIGITAL IMAGE CORRELATION FOR
DEFORMATION MEASUREMENTS
NEAR A CRACK**

Thesis Approved:



Thesis Advisor



Dean of the Graduate College

ACKNOWLEDGEMENTS

First and the foremost, I would like to thank Dr. Hongbing Lu, for his excellent guidance, inspiration and friendship without which this work would not have been possible. I am grateful for your patience and support throughout my studies in OSU.

I extend my sincere gratitude to the members of my advisory committee, Dr. Ranga Komanduri and Dr. Gary Young for finding time in their busy schedule. I would like to thank Dr. Bo Wang for his helpful suggestions and ideas whenever needed.

Further, I wish to thank my parents and my sister for their understanding, love and support throughout my stay away from home.

I would like to thank Mr. Harish Viswanathan, Mr. Gyuho Kim and all other weblab people for helping me in my research, by creating a pleasant working atmosphere. Finally, I would like to thank the School of Mechanical and Aerospace Engineering for supporting me during my M.S program.

TABLE OF CONTENTS

Chapter	Page
1.INTRODUCTION.....	1
1.1.Introduction to Digital Image Correlation	1
1.2.Overview of Digital Image Correlation Method.....	2
1.2.1.Application of Speckles	3
1.2.2.Image Acquisition	4
1.2.3.Correlation Method	5
1.3.Thesis Outline	8
2.THEORY BEHIND IMAGE CORRELATION	10
2.1.Effects of Mapping Parameters on Subset Around Node	10
2.2.Bicubic Spline Interpolation	12
2.3.Correlation Method.....	13
2.3.1. Least Squares Correlation Coefficient.....	13
2.3.2. Newton-Raphson Method	14
2.4.Processing of Subsequent Nodes.....	17
3.DIGITAL IMAGE CORRELATION FOR DEFORMATION MEASUREMENTS NEAR A CRACK	18
3.1.Solutions for Problems Encountered When Specimens had Cracks.....	19
3.1.1.Crack Detection by Connected Component Labeling	19
3.1.2.Procedure	20

Chapter	Page
3.1.3. Conversion of 8-bit grayscale image to binary image	20
3.1.4. Thresholding an image	21
3.1.5. Identifying Connected Components on a binary image	23
3.2. Modification to the Grayscale Interpolation and Least Square Correlation Algorithm to Account for Cracks	24
3.3. DeformedImageMaker Program	26
3.4. Results from New Algorithm	27
4. COMPUTATION OF J-INTEGRAL	29
4.1. J-integral	29
4.2. Calculation of J-integral Around Crack Tips	31
4.3. Theories Used for the Calculation of Stress	33
4.3.1. Linear Elastic Model	34
4.3.2. Ramberg-Osgood Model	34
4.3.3. Bilinear Model	36
4.4. Validation of J integral Algorithm Using Ideal Images	38
4.5. J integral for Actual specimens	42
4.5.1. Uniaxial Tensile Test on Rubbery Particulate Composite	42
4.5.2. Test results from materials which obey bilinear model	44
4.5.2.1. Particulate Composite Specimen Tested at 20% Pre-strain	44
4.5.2.2. Particulate Composite Specimen Tested at 15% Pre-strain	46
5. VALIDATION OF ALGORITHM USING NANOCOMPOSITE SPECIMENS	48
5.1. Background on nanocomposites	48
5.2. Specimen preparation	49

Chapter	Page
5.3.Experimental setup	50
5.4.Experimental procedures	52
5.5.Results and Discussion	52
6.CONCLUSIONS.....	56
REFERENCES.....	57
APPENDIXES	59
APPENDIX A – WinDIC_LS User’s Guide.....	60
APPENDIX B – Flow of Code for WinDIC.....	74
APPENDIX C – Flow of Code for J-integral Computation.....	76
APPENDIX D – DeformedImageMaker User’s Guide	77
APPENDIX E – Images Used in Uniaxial Tensile Test on Particulate Composites	79
APPENDIX F – Images of Particulate Composite Used in 20% Pre-Strain Test.....	81
APPENDIX G – Images of Particulate Composite Used in 15% Pre-Strain Test	83

LIST OF TABLES

Table	Page
4.1.Results for theoretical images.....	40
4.2.J integral (KPa -m) values for Uniaxial Tensile Test on Particulate Composite	42
4.3.Stress Intensity Factor Values for Uniaxial Tensile Test on Particulate Composite ..	43
4.4.J-integral (Kpa-m) values for 20% Pre-strain Test	45
4.5.J-integral (KPa-m) values for 15% Pre-strain Test	47
5.1.Fracture Toughness Values of samples	53

LIST OF FIGURES

Figure	Page
1.1.Naturally occurring speckle patterns.....	4
1.2.Speckle patterns generated by spraying paint	4
1.3.Image acquisition setup.....	5
1.4.Simplified demonstration of DIC.....	6
1.5.Grid of nodes to be placed on reference image.....	7
1.6.Reference image with reference grid on it	7
1.7.Deformed image with grid on it.....	8
2.1.Bicubic Spline Interpolation for grayscale data	12
3.1.Image of a specimen with crack	18
3.2.Image with unconverged nodes around crack	19
3.3.Input image.....	21
3.4.Binary image threshold = 69	21
3.5.Binary image threshold = 25	22
3.6.Binary image threshold = 106.....	22
3.7.Identification of independent regions.....	23
3.8.Cracked specimen with grid of nodes	25
3.9.Nodes lying in the crack had been removed	25
3.10.Bicubic Interpolation for modified correlation	26
3.11.Theoretical image used for computation.....	27

3.12.Theoretical image with nodal grid placed on it.....	28
3.13.Theoretical image with nodes falling in to the crack removed	28
4.1.J-integral contour.....	30
4.2.Direction of right outward normal	32
4.3.Direction of left outward normal.....	33
4.4.Reference ideal image	41
4.5.Deformed Ideal image.....	41
4.6.Plot of K Vs Distance for uniaxial tensile test on particulate composite	44
4.7.Stress-strain curve for 20% pre-strain test	45
4.8.Stress-strain curve for 15% pre-strain test	46
5.1.Specimen dimensions.....	49
5.2.Three-point bending specimen	50
5.3.Instron machine setup.....	51
5.4.Reference image.....	52
5.5.Deformed image.....	52
5.6.Strain distribution nanocomposite specimen with 3% nanoclay loading.....	54

NOMENCLATURE

U_0, V_0	translation mapping parameters; $u(x, y), v(x, y)$.
U_x, V_x	first order mapping gradients; $\frac{\partial u}{\partial x}(x, y), \frac{\partial v}{\partial x}(x, y)$.
U_y, V_y	first order mapping gradients; $\frac{\partial u}{\partial y}(x, y), \frac{\partial v}{\partial y}(x, y)$.
U_{xx}, V_{xx}	second order mapping gradients; $\frac{\partial^2 u}{\partial x^2}(x, y), \frac{\partial^2 v}{\partial x^2}(x, y)$.
U_{yy}, V_{yy}	second order mapping gradients; $\frac{\partial^2 u}{\partial y^2}(x, y), \frac{\partial^2 v}{\partial y^2}(x, y)$.
U_{xy}, V_{xy}	second order mapping gradients; $\frac{\partial^2 u}{\partial x \partial y}(x, y), \frac{\partial^2 v}{\partial x \partial y}(x, y)$.
w	height or grayscale value offset.
\mathbf{P}	represents all thirteen mapping parameters.
S	represents all points in subset around a node.
S_p	represents a single point in the subset at location (x, y) .
x, y	subset point location in reference image.
\tilde{x}, \tilde{y}	Subset point location in deformed image.
$\Delta x, \Delta y$	distance from node to subset point

$C, \nabla C, \nabla \nabla C$ least square correlation coefficient, gradient, and Hessian (second gradient).

$\delta x, \delta y$ distance from current node to next node.

$\varepsilon_1, \varepsilon_2$ principal strains.

CHAPTER 1

INTRODUCTION

1.1. Introduction to Digital Image Correlation

Digital Image Correlation (DIC) is a method for measurements of surface displacements and displacement gradients in materials under deformation. It is a non-contact, full field deformation measurement method that can be used in a variety of situations that include high temperature situations. It is also appropriate for relatively soft materials where strain gauges are not appropriate for deformation measurement. The method is applicable for both infinitesimal and large deformations. It was originally proposed by a group of researchers at the University of South Carolina (Peters and Ranson, 1982, Sutton, et al, 1983 and Bruck, et al, 1989). Later work has been done by Knauss and Vendroux (1998), to refine and optimize the basic algorithms for use in in-plane and out-of plane deformation measurements.

Recently Lu and Cary (2000), extended the previous DIC methods by accounting for the second order displacement gradients. Ganesan (2001), has included third order terms in the deformation mapping. This higher order approximation provides a better measurement of infinitesimal strain in relatively non-linear deformation situations. It has also provided a method to measure first and second order strain gradients. However problems were encountered in obtaining deformation data near a crack. The reason behind this is the inability of the present algorithm to converge near the crack tip.

Sutton et al., (1991), have reported a reduced accuracy in determining J-integral around a crack. They attribute this reduced accuracy in determining the path independent J-integral to the inability of finding the displacements close to the crack. Knauss and Gonzalez (1998) have reported the same shortcoming when using DIC to study the inhomogeneity in particulate composites.

This thesis work describes the methods to overcome this difficulty. The algorithm will first detect the crack edges and then take into account, the presence of the crack in deformation measurements through image correlation. The crack is detected by the method of Connected Component Labeling. After the crack is detected the nodes falling into the crack region are excluded in DIC for displacement computations. An algorithm for finding the J-integral for linear elastic materials, materials obeying Ramberg-Osgood model, and bilinear materials are also proposed. The proposed methods are validated by performing correlation on theoretical images generated using Deformed image maker program. Results obtained for rubbery particulate composites are also presented. Experimental images acquired in three-point bending tests on Epoxy nanocomposite specimens with cracks are also presented to validate the DIC.

1.2.Overview of Digital Image Correlation Method

There are three steps involved in carrying out DIC method to correlate two images, one undeformed and one deformed to determine deformation field. They are:

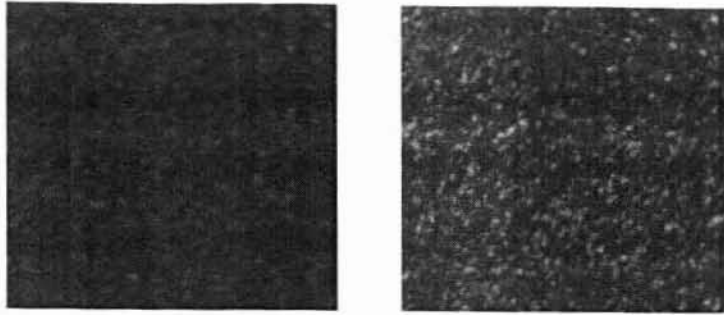
- (1). Application of speckles to the specimen, it is noted that for specimens already possessing surface gray scale patterns, no surface treatment is required. In micro- and nano-scale deformation measurements, the polished surface followed by chemical etching produce sufficient gray scale pattern for DIC.

(2). Image Acquisition. On a macroscopic scale a digital camera can be used to acquire images. On micro-scale an optical microscope or an SEM can be used to acquire micrographs. On nano-scale AFM or TEM or other microscopy instrument can be used to acquire images representing surface topology or surface gray scale.

(3). Correlation of reference and deformed images. Using the code developed from an appropriate algorithm, in this study, a code named WinDIC developed in Dr.Lu's laboratory is used. In the sequel a detailed description of these steps is provided.

1.2.1.Application of Speckles

For computing the deformations some random texture or patterns are needed on the specimens. These are called speckles. Some specimens have naturally occurring speckles so that images of the specimen surface can be used for correlation directly. Figure 1.1(a) shows some naturally occurring speckle patterns on rubbery particulate composites and Figure 1.1(b) is that of nanocomposites. Some specimens do not have naturally occurring speckle pattern. Then the speckles for such specimens are to be applied manually. The speckles can be generated by spraying paint by holding the paint can at a distance. Figure 1.2 shows the speckle patterns generated by spraying paint. Care should be taken to see that the paint creates speckles with random gray scale pattern. The speckle size should be optimized so that each speckle has a characteristic length of about a few pixels. The density of the speckle pattern should be high enough for the accurate correlation process of a gray scale pattern around a point. Locating a subset of points found on the reference image, in the deformed image, carries out the mapping of a point on the reference image on to the deformed image. This is the reason for having a random pattern of points on the specimen surface.



(a) Rubbery particulate Composite. (b) Nanocomposite.

Figure 1.1: Naturally occurring speckle patterns.

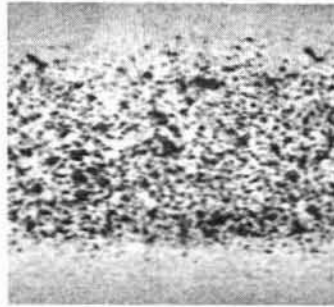


Figure 1.2: Speckle patterns generated by spraying paint.

1.2.2. Image Acquisition

The image acquisition system used in this study consists of a Kodak-ES camera mounted on a tripod. The camera is connected to a computer, which has the software for acquiring images of the specimen as the test proceeds. A Techniquip Corp, R 150 A2 fibre optic light source is used to illuminate the specimen surface so as to enable the camera to capture the image. Figure 1.3 shows the image acquisition set up for capturing images of specimen during test.

The software used for capturing images is called "CAPTURE". This software has provisions for capturing the images at regular intervals of time. A total of 99 images can be captured for one timer file. The software starts capturing the images once the trigger is

given by striking a key. Once the timer is set, the images will be acquired automatically.

Thus the images for the image correlation procedure are captured.

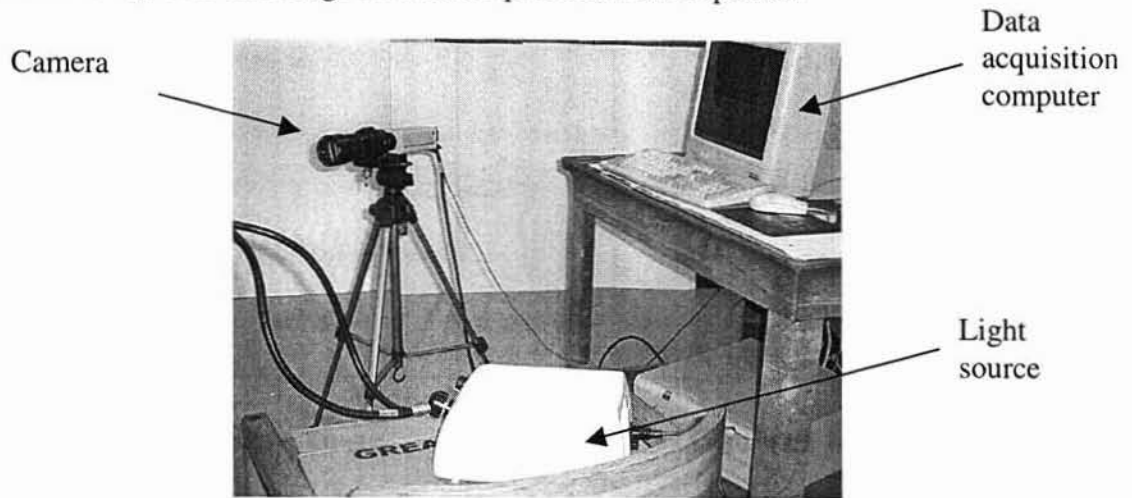


Figure 1.3: Image acquisition setup

1.2.3. Correlation Method

DIC method uses two images of the specimen under deformation for correlation. The images are the reference and deformed images. The reference image is the image acquired in the undeformed state. Deformed image is the image acquired after the specimen has undergone deformation. Figure 1.4 illustrates how the correlation of two images is carried out. Let A be a point on the reference image, which moves to point B in the deformed image. The displacements in the X and Y directions are U and V respectively. These displacements are for one particular point on the specimen. If the deformation along the surface of the specimen is to be observed a number of points in the form of a grid can be placed on the reference image. Each point on the reference grid can be mapped from reference image to the deformed image to get the deformation along the surface of the specimen. So the reference grid placed on the reference image deforms to different shapes for a deformation value of 1.0 for different deformation gradients.

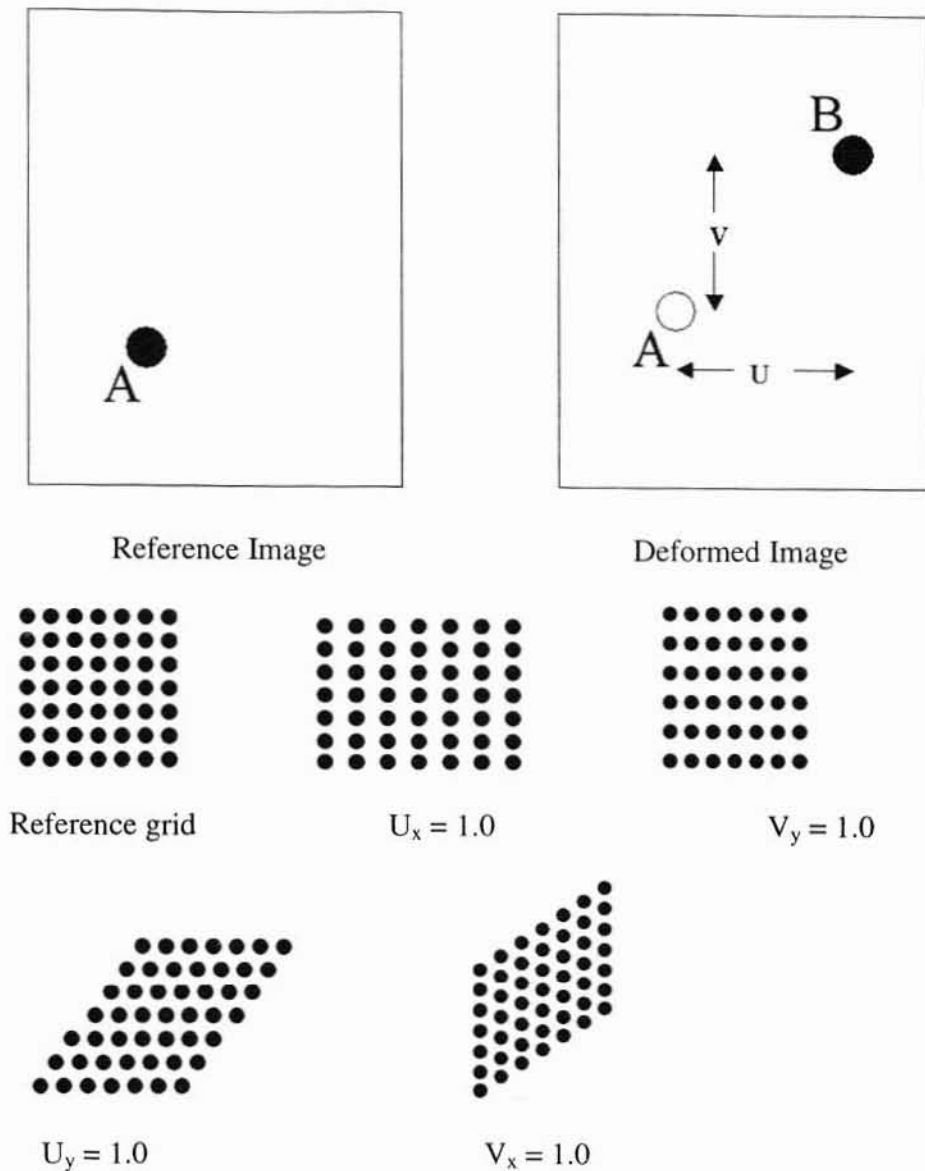


Figure 1.4: Simplified demonstration of DIC.

DIC is carried out by comparing the deformed image with the reference image. There exists a distinct grayscale pattern around a point where deformation will be computed. The grayscale pattern can shrink, expand or rotate, but the basic shape does not change in the deformed image after the deformation. By tracking the movement of the unique grayscale pattern on the deformed image the deformation can be determined. This process is performed by a code using DIC algorithm described in Chapter 2.

A set of points, or equivalent nodes, is needed on both images to carry out correlation. A grid of nodes is placed on the reference image and a mapping is performed on each of these nodes to capture the same point on the deformed image. Figure 1.5 shows a grid of nodes that is placed on the reference image to carry out the correlation on the deformed images.

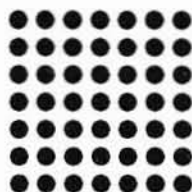


Figure 1.5: Grid of nodes to be placed on reference image.

The number of nodes in the grid can be changed according to the extent of the correlation to be carried out on the specimen. Figure 1.6 shows the reference image with the grid on it before the correlation is carried out. The grid of nodes have to be placed on the reference image in such a way that the grid is totally on the image of the specimen.

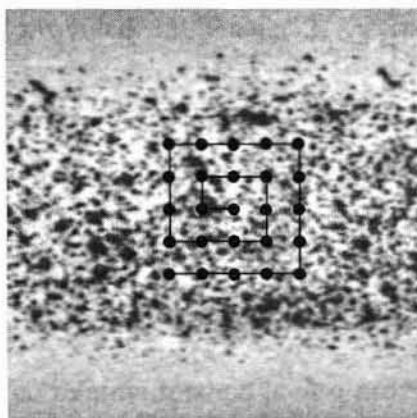


Figure 1.6: Reference image with reference grid on it.

Figure 1.7 shows the deformed image with the deformed grid after the correlation has been carried out. A set of points around a node in the grid is considered.

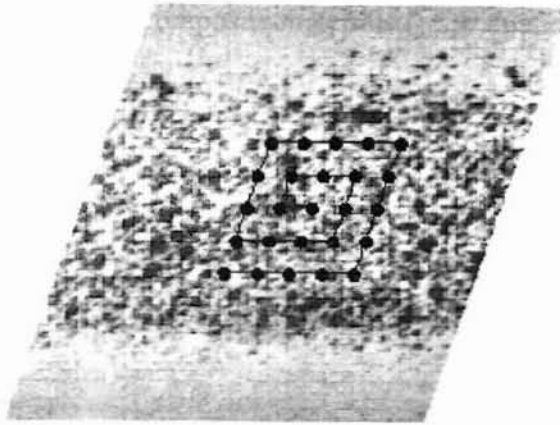


Figure 1.7: Deformed image with grid on it.

Using these random points a particular node is identified on the deformed image. This is repeated for each and every node on the grid. The fundamental level of calculation is at the node level, so the whole algorithm is for each node.

1.3.Thesis Outline

In Chapter1, an introduction to the DIC and a simplified demonstration of the correlation process has been provided. In Chapter 2, a detailed discussion of the theory behind DIC is provided. Discussion on least squares correlation coefficient; Newton-Raphson method and bicubic spline interpolation method is provided. Chapter 3 presents a discussion on the problems experienced with DIC when used for specimens with cracks and a method to overcome the problems associated with such specimens. A detailed explanation of the modified correlation method is also provided. Chapter 4 discusses the J-integral calculation approach and the results obtained with DIC for particulate composites in various test conditions. Chapter 5 discusses the results obtained from three-point bending tests conducted on Epoxy nanocomposites to validate the improved algorithm for deformation measurements are provided. From the results it was found that

the algorithm could be used for nanocomposite materials for evaluation of strain. Chapter 6 lists the conclusions based on the current study.

CHAPTER 2

THEORY BEHIND IMAGE CORRELATION

This chapter deals with the theory for DIC. The interpolation techniques and the correlation using Newton-Raphson method, the two major steps in DIC, are explained in detail.

2.1. Effects of Mapping Parameters on Subset Around Node

A subset of points around a node is used for measurement of displacements for the node. Let us consider a subset of points around a node that is mapped from the reference image to the deformed image. Each of these subset points is located in the reference image at (x, y) and is mapped to the deformed image at location (\tilde{x}, \tilde{y}) using

$$\tilde{x} = x + U(x, y),$$

$$\tilde{y} = y + V(x, y)$$

where U is the displacement in the x direction and V is the displacement in the y direction of each subset point. The terms U and V when approximated using first order Taylor series expansion around a point (x_0, y_0) leads to the following mapping functions

$$\tilde{x} = x + U_0 + U_x \Delta x + U_y \Delta y,$$

$$\tilde{y} = y + V_0 + V_x \Delta x + V_y \Delta y$$

where

$$\Delta x = x - x_0,$$

$$\Delta y = y - y_0.$$

U_x, V_x, U_y, V_y are in-plane components of the first order displacement gradient. The two terms U_0 and V_0 are displacement components of (x_0, y_0) . There are seven mapping parameters involved in the first order Taylor series expansion they are $U_0, V_0, U_x, V_x, U_y, V_y$ and w . Likewise there are mapping parameters calculated for second order and third order Taylor series to compute the deformation of the specimen.

The second order Taylor series approximation was carried out by Lu and Cary, 2000. The terms U and V when approximated using second order Taylor series expansion around a point (x_0, y_0) leads to the following mapping functions.

$$\begin{aligned}\tilde{x} &= x + U_0 + U_x \Delta x + U_y \Delta y + \frac{1}{2} U_{xx} \Delta x^2 + \frac{1}{2} U_{yy} \Delta y^2 + U_{xy} \Delta x \Delta y, \\ \tilde{y} &= y + V_0 + V_x \Delta x + V_y \Delta y + \frac{1}{2} V_{xx} \Delta x^2 + \frac{1}{2} V_{yy} \Delta y^2 + V_{xy} \Delta x \Delta y\end{aligned}$$

There are thirteen mapping parameters involved in the second order Taylor series expansion, they are $U_0, V_0, U_x, V_x, U_y, V_y, U_{xx}, V_{xx}, U_{yy}, V_{yy}, U_{xy}, V_{xy}$ and w .

Likewise the third order Taylor series approximation carried out by Ganesan (2001), leads to the following mapping functions,

$$\begin{aligned}\tilde{x} &= x + U_0 + U_x \Delta x + U_y \Delta y + \frac{1}{2} U_{xx} \Delta x^2 + \frac{1}{2} U_{yy} \Delta y^2 + U_{xy} \Delta x \Delta y + \frac{1}{6} U_{xxx} \Delta x^3 \\ &+ \frac{1}{6} U_{yyy} \Delta y^3 + \frac{1}{2} U_{xxy} \Delta x^2 \Delta y + \frac{1}{2} U_{yyx} \Delta y^2 \Delta x \\ \tilde{y} &= y + V_0 + V_x \Delta x + V_y \Delta y + \frac{1}{2} V_{xx} \Delta x^2 + \frac{1}{2} V_{yy} \Delta y^2 + V_{xy} \Delta x \Delta y + \frac{1}{6} V_{xxx} \Delta x^3 \\ &+ \frac{1}{6} V_{yyy} \Delta y^3 + \frac{1}{2} V_{xxy} \Delta x^2 \Delta y + \frac{1}{2} V_{yyx} \Delta y^2 \Delta x\end{aligned}$$

There are twenty three mapping parameters involved in the third order Taylor series expansion, they are $U_0, V_0, U_x, V_x, U_y, V_y, U_{xx}, V_{xx}, U_{yy}, V_{yy}, U_{xy}, V_{xy}, U_{xxx}, V_{xxx}, U_{yyy}, V_{yyy}, U_{xxy}, V_{xxy}, U_{yyx}, V_{yyx}, W, W_x$ and W_y .

2.2. Bicubic Spline Interpolation

The images are interpolated using bicubic spline interpolation to achieve sub-pixel accuracy. Figure 2.1 shows a bicubic spline surface, Sutton, Turner et al (1991), that has been interpolated through a set of image pixel grayscale values. The interpolation technique uses a third order polynomial to determine grayscale values at locations between the pixel locations; the third order polynomial has a C^2 continuous gradients of the grayscale value field.

The grayscale value at any location in the interpolated region of the reference image can be calculated using the equation,

$$g(x, y) = \sum_{m=0}^3 \sum_{n=0}^3 \alpha_{mn} x^m y^n$$

where α_{mn} are the coefficients of the bicubic spline interpolation. They are determined by using the grayscale values of the corner points of any rectangular surface patch on the bicubic surface.

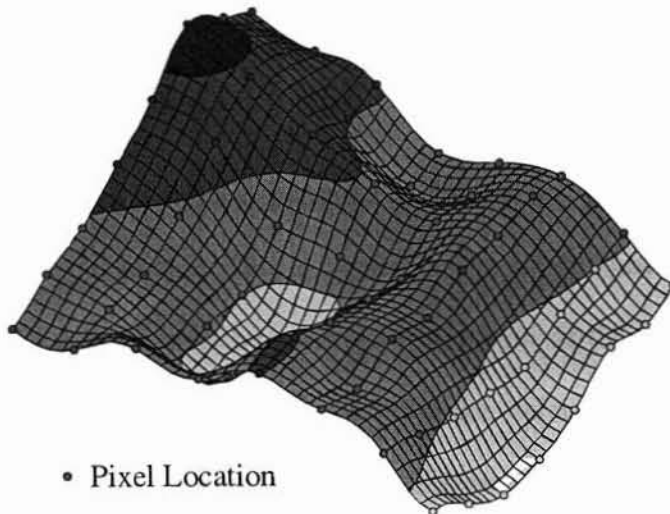


Figure 2.1: Bicubic spline interpolation for image grayscale data

The thirteenth mapping parameter w comes in the form of a grayscale value offset of the bicubic spline interpolation for the deformed image. This is introduced to compensate for the errors introduced by changes in the light intensities when the images are acquired for image correlation.

$$h(\tilde{x}, \tilde{y}, P) = \sum_{m=0}^3 \sum_{n=0}^3 \beta_{mn} \tilde{x}^m \tilde{y}^n + w$$

For later simplification, let P represent a vector with all thirteen mapping parameters as its components (in case of second order Taylor series being used). The number of mapping parameters depends on the order of the Taylor series used to carry out the approximation. For second order Taylor series approximation,

$$P = \{U_0, V_0, U_x, V_x, U_y, V_y, U_{xx}, V_{xx}, U_{yy}, V_{yy}, U_{xy}, V_{xy}, w\}$$

The gradients are needed to carry out the correlation process, where the minimization of the least squares correlation coefficient is carried out to find the mapping parameters.

2.3. Correlation Method

2.3.1. Least Squares Correlation Coefficient

The values of the mapping parameters are to be determined to obtain the deformation values in the sample. This is carried out by Least squares correlation. Least squares correlation method works by minimizing the sum of the squares of the errors. Here in this case the difference between the grayscale values of the reference and the deformed image is taken as the error. When this difference tends to zero the point on the reference image can be reached on the deformed image. Let S represent all the points in the subset and S_p represent any single point in the subset. Let $g(S_p)$ represents the

grayscale value of a particular point in the subset on the reference image and $h(S_p)$ represents the grayscale value of the same point in the subset on the deformed image. Then correlation coefficient is defined as

$$C = \frac{\sum_{S_p \in S} \{g(S_p) - h(S_p, S)\}^2}{\sum_{S_p \in S} g^2(S_p)}$$

The summations are performed over all the points of the subset region. From the equation the range of values for C is from $[0, \infty]$, where the optimum value of C is reached when $g \approx h$ which leads to $c \approx 0$. The set of P, which minimizes the correlation coefficient C, are in fact the parameters of the mapping caused by the deformation in the sample.

To find the minimum of C all the gradients of C must converge to zero. The thirteen gradients of C are

$$(\nabla C)_i = \frac{\partial C}{\partial P_i} = \frac{-2}{\sum_{S_p \in S} g^2(S_p)} \left\{ \sum_{S_p \in S} (g(S_p) - h(S_p, P)) \frac{\partial h(S_p, P)}{\partial P_i} \right\}$$

The Newton-Raphson method can be used to solve for the roots of these gradients simultaneously.

2.3.2. Newton-Raphson Method

Newton-Raphson method is an iterative procedure for finding the roots of an equation. It requires initial guesses for variables that are to be determined. A set of linear equations must be solved using the initial guess for equations of the form,

$$X_{n+1} = X_n - \frac{f(X_n)}{f'(X_n)}$$

$f(X_n)$ is the value of the gradients (∇C) at the current location. $f'(X_n)$ is the value of $\nabla \nabla C$ at the current location. User supplies the initial guess for the mapping parameters of the first node. The X_{n+1} are the increment values for the next location. In the present case the roots are being determined for the gradient of the correlation coefficient, ∇C . The $\nabla \nabla C$ is called the Hessian matrix of the correlation coefficient.

The Crout Lu (Gerard, Wheatley, 1994) decomposition method is used to solve the set of linear equations. Subsequent nodes use the results from the previous node as the guess values. The Hessian matrix of the correlation coefficient is given by,

$$\nabla \nabla C = \frac{\partial^2 C}{\partial P_i \partial P_j} = \frac{-2}{\sum_{S_p \in S} g^2(S_p)} \sum_{S_p \in S} (g(S_p) - h(S_p, P)) \frac{\partial^2 h(S_p, P)}{\partial P_i \partial P_j} + \frac{2}{\sum_{S_p \in S} g^2(S_p)} \sum_{S_p \in S} \frac{\partial h(S_p, P)}{\partial P_i} \frac{\partial h(S_p, P)}{\partial P_j}$$

$g(x,y) \approx h(x,y,P)$ when the initial guesses for P are close to the actual solution then we can make the following approximation,

$$\sum_{S_p \in S} (g(S_p) - h(S_p, P)) \frac{\partial^2 h(S_p, P)}{\partial P_i \partial P_j} \approx 0$$

Then the Hessian matrix of the correlation coefficient can be approximated as,

$$\nabla \nabla C = \frac{2}{\sum_{S_p \in S} g^2(S_p)} \sum_{S_p \in S} \frac{\partial h(S_p, P)}{\partial P_i} \frac{\partial h(S_p, P)}{\partial P_j}$$

The approximate Hessian matrix is sufficient in this case because we assume that the initial guesses for P are close to the actual solution. The partial derivatives of the grayscale values are functions of both the displacement mapping and the bicubic

interpolation of the deformed image pixel values. The partial derivatives can be evaluated using the chain rule,

$$\frac{\partial h(S_p, P)}{\partial P_i} = \frac{\partial h(\tilde{x}, \tilde{y}, P)}{\partial \tilde{x}} \cdot \frac{\partial \tilde{x}(S_p)}{\partial P_i} + \frac{\partial h(\tilde{x}, \tilde{y}, P)}{\partial \tilde{y}} \cdot \frac{\partial \tilde{y}(S_p)}{\partial P_i} + \frac{\partial h(\tilde{x}, \tilde{y}, P)}{\partial P_i}$$

The equations for calculating the partial derivatives for $\frac{\partial h(S_p, P)}{\partial P_i}$, using second

order deformation gradient, for each point S_p are as follows,

$$\begin{aligned} \frac{\partial h}{\partial U} &= \frac{\partial h}{\partial \tilde{x}} & \frac{\partial h}{\partial V} &= \frac{\partial h}{\partial \tilde{y}} & \frac{\partial h}{\partial U_x} &= \frac{\partial h}{\partial \tilde{x}} \Delta x & \frac{\partial h}{\partial V_x} &= \frac{\partial h}{\partial \tilde{y}} \Delta x \\ \frac{\partial h}{\partial U_y} &= \frac{\partial h}{\partial \tilde{x}} \Delta y & \frac{\partial h}{\partial V_y} &= \frac{\partial h}{\partial \tilde{y}} \Delta y & \frac{\partial h}{\partial U_{xx}} &= \frac{1}{2} \frac{\partial h}{\partial \tilde{x}} \Delta x^2 & \frac{\partial h}{\partial V_{xx}} &= \frac{1}{2} \frac{\partial h}{\partial \tilde{y}} \Delta y^2 \\ \frac{\partial h}{\partial U_{yy}} &= \frac{1}{2} \frac{\partial h}{\partial \tilde{x}} \Delta y^2 & \frac{\partial h}{\partial V_{yy}} &= \frac{1}{2} \frac{\partial h}{\partial \tilde{y}} \Delta y^2 & \frac{\partial h}{\partial U_{xy}} &= \frac{\partial h}{\partial \tilde{x}} \Delta x \Delta y & \frac{\partial h}{\partial V_{xy}} &= \frac{\partial h}{\partial \tilde{y}} \Delta x \Delta y \\ \frac{\partial h}{\partial w} &= 1 \end{aligned}$$

The equations for calculating the partial derivatives for $\frac{\partial h(S_p, P)}{\partial P_i}$, using third

order deformation gradient, for each point S_p are as follows,

$$\begin{aligned} \frac{\partial h}{\partial U_{xxx}} &= \frac{1}{6} \frac{\partial h}{\partial \tilde{x}} \Delta x^3 & \frac{\partial h}{\partial V_{xxx}} &= \frac{1}{6} \frac{\partial h}{\partial \tilde{y}} \Delta x^3 & \frac{\partial h}{\partial U_{yyy}} &= \frac{1}{6} \frac{\partial h}{\partial \tilde{x}} \Delta y^3 & \frac{\partial h}{\partial V_{yyy}} &= \frac{1}{6} \frac{\partial h}{\partial \tilde{y}} \Delta y^3 \\ \frac{\partial h}{\partial U_{xxy}} &= \frac{1}{2} \frac{\partial h}{\partial \tilde{x}} \Delta x^2 \Delta y & \frac{\partial h}{\partial V_{xxy}} &= \frac{1}{2} \frac{\partial h}{\partial \tilde{y}} \Delta x^2 \Delta y & \frac{\partial h}{\partial U_{yyx}} &= \frac{1}{2} \frac{\partial h}{\partial \tilde{x}} \Delta x \Delta y^2 & \frac{\partial h}{\partial V_{yyx}} &= \frac{1}{2} \frac{\partial h}{\partial \tilde{y}} \Delta x \Delta y^2 \\ \frac{\partial h}{\partial w_x} &= \Delta x & \frac{\partial h}{\partial w_y} &= \Delta y & \frac{\partial h}{\partial w} &= 1 \end{aligned}$$

The $\frac{\partial h}{\partial \tilde{x}}$ and $\frac{\partial h}{\partial \tilde{y}}$ terms of these partial derivatives are the gradients of the bicubic spline interpolating polynomial from the deformed image,

$$\begin{aligned} \frac{\partial h}{\partial \tilde{x}} = & \beta_{21} + \beta_{22}\tilde{y} + \beta_{23}\tilde{y}^2 + \beta_{24}\tilde{y}^3 + 2\beta_{31}\tilde{x} + 2\beta_{32}\tilde{x}\tilde{y} + 2\beta_{33}\tilde{x}\tilde{y}^2 + 2\beta_{34}\tilde{x}\tilde{y}^3 + 3\beta_{41}\tilde{x}^2 \\ & + 3\beta_{42}\tilde{x}^2\tilde{y} + 3\beta_{43}\tilde{x}^2\tilde{y}^2 + 3\beta_{44}\tilde{x}^2\tilde{y}^3, \end{aligned}$$

$$\begin{aligned} \frac{\partial h}{\partial \tilde{y}} = & \beta_{12} + 2\beta_{13}\tilde{y} + 3\beta_{14}\tilde{y}^2 + \beta_{22}\tilde{x} + 2\beta_{23}\tilde{x}\tilde{y} + 3\beta_{24}\tilde{x}\tilde{y}^2 + \beta_{32}\tilde{x}^2 + 2\beta_{33}\tilde{x}^2\tilde{y} + 3\beta_{34}\tilde{x}^2\tilde{y}^2 \\ & + \beta_{42}\tilde{x}^3 + 2\beta_{43}\tilde{x}^3\tilde{y} + 3\beta_{44}\tilde{x}^3\tilde{y}^2. \end{aligned}$$

2.4. Processing of Subsequent Nodes

After the minimization of the correlation coefficient is done, the process is repeated using the next node location on the grid of nodes. The values obtained in the previous calculations are used as the initial guesses for the next node, but the previous values of the displacements U_0 and V_0 are adjusted for the next node's guesses using the deformation equations

$$U_{0n} = U_0 + U_x \Delta x + U_y \Delta y + \frac{1}{2} U_{xx} \Delta x^2 + \frac{1}{2} U_{yy} \Delta y^2 + U_{xy} \Delta x \Delta y,$$

$$V_{0n} = V_0 + V_x \Delta x + V_y \Delta y + \frac{1}{2} V_{xx} \Delta x^2 + \frac{1}{2} V_{yy} \Delta y^2 + V_{xy} \Delta x \Delta y.$$

where

$$\Delta x = x - x_0, \Delta y = y - y_0.$$

More closer the guess as to the location of the next node in the deformed image can be made if the above adjustment can be added into the next node's initial translation parameter values.

CHAPTER 3

DIGITAL IMAGE CORRELATION FOR DEFORMATION MEASUREMENTS NEAR A CRACK

When DIC is used on specimens without cracks the results for displacement gradients are accurate. All the nodes placed on the deformed images can normally converge very well. Problems arose when the correlation was used on specimens with cracks on them. The nodes do not converge and the results obtained are inaccurate. Figure 3.1 shows an image of the specimen with a crack on it. The specimen used is rubbery particulate composite. Resolution of the image is 512x486 pixels. The width of the actual specimen is 1 inch. The image has 166 pixels per meter which is the conversion factor used for the calculation of J-integral.

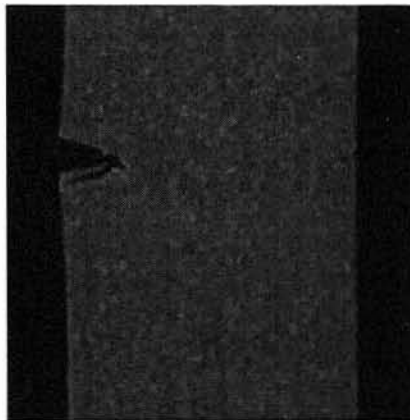


Figure 3.1: Image of a specimen with crack

The following problems are often encountered in DIC in the vicinity of a crack.

1) The nodes surrounding the cracks did not converge and so the deformation results could not be obtained in those regions. Figure 3.2 shows the image of the specimen with the deformed nodal grid on it. There are a number of unconverged nodes surrounding the crack. This is because the present algorithm has not considered the nodes in the crack area and is unable to converge to solutions for the nodes near the crack edges.

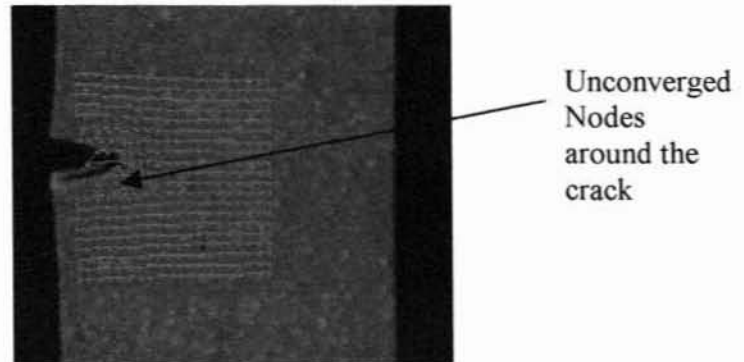


Figure 3.2: Image with unconverged nodes around crack

2) The calculation of J-integral around cracks was affected because of the non-convergence of nodes around crack, as the J-integral computation depends upon the displacement results for each node that lies along a path chosen for J-integral computation.

3.1.Solutions for Problems Encountered When the Specimen had Cracks

3.1.1.Crack Detection by Connected Component Labeling

The aim of this process is to identify and mark or label independent connected regions. Connected components labeling is a method by which an image is scanned and pixels are grouped into components based on pixel connectivity. The pixels in a component share similar pixel intensity values. After grouping the pixels, each of the pixels is labeled with either of the two colors, black or white. Once the grouping is done

the regions with black pixels are extracted. This forms a connected component and that is the crack in this case. The method used to detect the crack relies on the fact that the crack appears as a region of either higher or lower grayscale as compared to its surrounding area. The image is first converted from a grayscale image to a binary image by the operation of thresholding the grayscale of an image. All pixels with a grayscale value above a certain threshold are made white and the ones with lesser grayscale black. Thus leading to connected components.

3.1.2.Procedure

An image is scanned pixel-by-pixel from top to bottom and left to right, so as to identify the connected regions. Connected regions are the adjacent pixels, which share the same intensity value v . For a binary image $v = \{1\}$, whereas for a grayscale image v can take a range of values for the different gray scales.

Connected component labeling method needs a binary image as input. In the case of DIC an 8-bit gray scale image is used. So it is to be converted into binary image by taking the black and white pixels on the image into consideration.

3.1.3.Conversion of 8-bit Grayscale Image to Binary Image

The method used to detect the crack relies on the fact that the crack appears as a region of either higher or lower grayscale as compared to its surrounding area. The image is first converted from a grayscale image to a binary image by the operation of thresholding the grayscale the image. All pixels with a grayscale values above a certain threshold are made white and the ones with lower grayscale values black. Thus black and white regions are identified on the image. The black and white regions are used to form

independent connected regions on the image, which will serve as the input for the Connected Component labeling.

3.1.4. Thresholding an Image

To threshold an image the user provides a particular grayscale value as the threshold value. A binary image has only two components of color namely black and white. Based on the threshold value the black and white components in an image are identified. The pixels with grayscale values less than the threshold values are taken as black and the pixels with grayscale values greater than the threshold value are taken as white. So when all the pixels on the image are replaced using this procedure, it results in an image with just two intensity values namely black and white. Thus a binary image is created from a grayscale image. Figure 3.3 shows an 8-bit grayscale image of the epoxy nanocomposite. The image captured by the camera is converted into 8-bit grayscale image with the help of Paint Shop Pro software. Figures 3.4 - 3.6 show the conversion of a grayscale image into binary images when different threshold values are chosen.

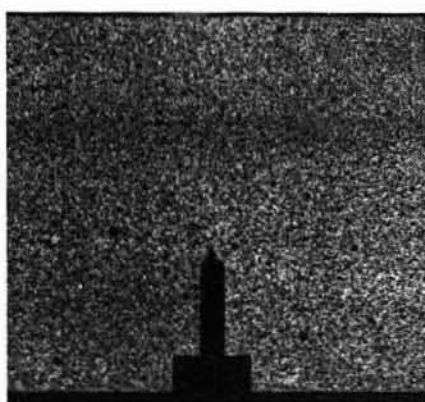


Figure 3.3: Input image

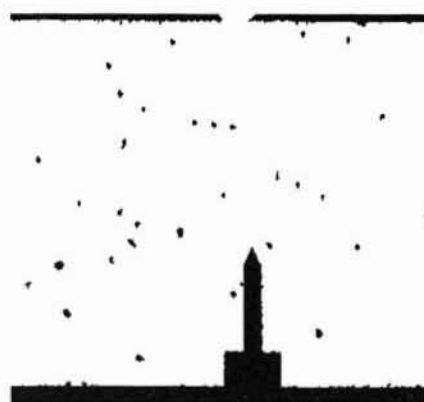


Figure 3.4: Binary image threshold = 69

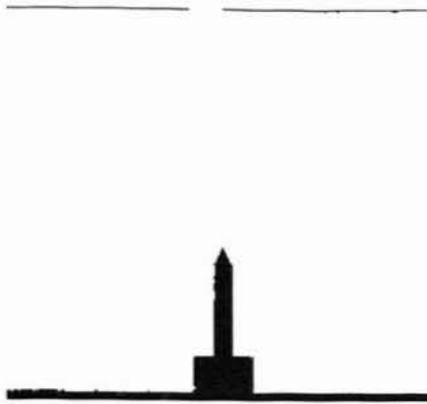


Figure 3.5: Binary image threshold = 25

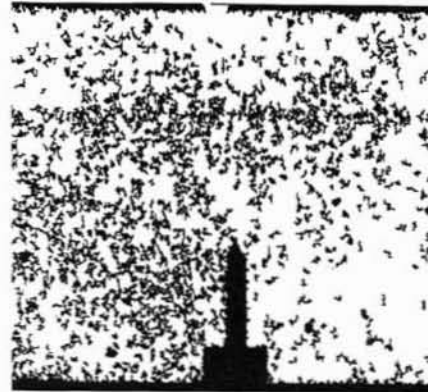


Figure 3.6: Binary image threshold = 106

Figure 3.4 shows the resulting image of Connected Component Labeling when the threshold value chosen is 69. There are some black spots left on the image. As there are many pixels on the image with grayscale values less than 69, many dark spots are formed on the image. Figure 3.5 shows an image that results when the threshold value is 25. It can be seen from the image that as the threshold value decreases the crack detection the resulting image has lesser number of black spots on it. Figure 3.6 shows an image with threshold value of 106. It can be seen that as the threshold value is high the image obtained does not result in good crack detection. The image shows a lot of black spots, which have to be removed in order to obtain images on figure 3.4 or figure 3.5. This can be achieved by either doing a rerun with different threshold value or with the erase option in the DIC software to remove the spots. An optimum value of threshold value must be chosen to obtain good results, which can be done by running the crack detection with different threshold values and selecting the value, which produces an image with lesser number of spots.

3.1.5. Identifying Connected Components on a Binary Image

The aim of this process is to identify and mark or label independent connected regions. A connected region is made of adjacent pixels that share the same intensity value. In this process, each pixel of the picture is assigned a number, also called a label. All pixels in a connected region are assigned the same label. The process works by scanning the image pixel by pixel, left to right, top to bottom. When a dark pixel p is encountered, two of its neighbors, one to the left of p and the one above p are examined. If both neighbors are white, a new label is assigned to p . If only one neighbor is dark, its label is assigned to p . If one or more of the neighbors are dark, one of the labels of the two neighbors is assigned to p and a note is made of the equivalence of labels of the two neighbors. After completing the scan, the equivalent label pairs are processed and a unique label is assigned to each connected region.

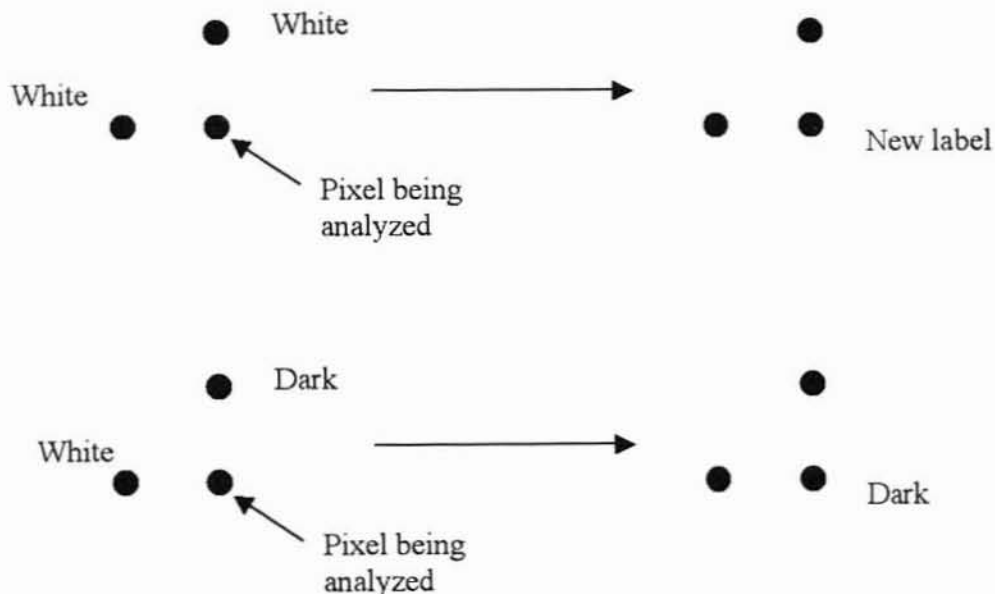


Figure 3.7: Identification of independent regions

The dark pixels, which are clustered in the fashion shown in the Figure 3.4 lead to many independent connected regions. The area of each independent connected region is determined by counting the number of pixels with the same label.

With this count of area for each label, all the pixels in the image whose label has an area less than a particular threshold area value are identified and removed. This will remove all the dark speckles, which are lesser in area compared to the crack, as the crack will have the largest independent connected region area, producing an image with just the crack

3.2.Modification to the Grayscale Interpolation and Least Square Correlation

Algorithm to Account for Cracks

The presence of crack in the subset region affects the mapping of the subset points on the reference image to that of the deformed image. As the crack is not a part of the material and as it does not deform just like any other material point in the subset, the algorithm does not converge for nodes that fall into the crack region. As the crack is not a part of the material, the nodes in the crack region will not have any deformation values. As the nodes in the crack do not dislocate to the same extent as those of the specimen, the algorithm does not converge to give accurate results. So they should not be taken into consideration for deformation computations. Modified correlation works by excluding all the points that lie in the crack region at each stage of iteration.

Figure 3.7 shows an example of a specimen with computation nodal grid. Note that there are some nodes into the crack region. In computation, the crack surface does not contribute to the deformation field. So the nodes in the crack region should be removed from the grid such that they are not taken into consideration of deformation

calculation. Figure 3.8 shows the specimen with the nodes lying in the crack region removed. So the present interpolation algorithm should be changed to account for the nodes removed from the subset.

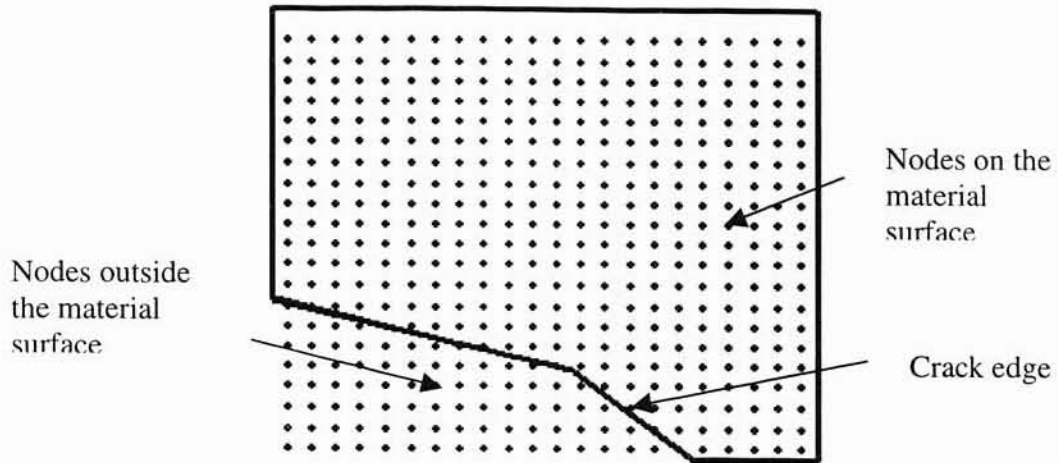


Figure 3.8: Cracked specimen with grid of nodes

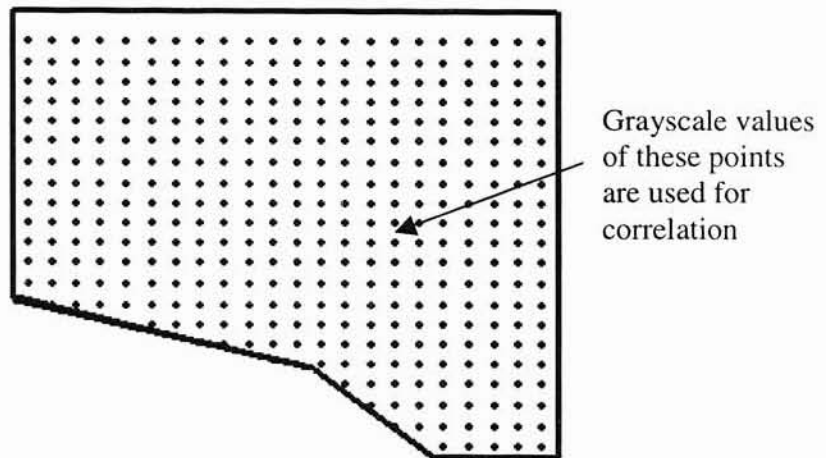


Figure 3.9: Nodes lying in the crack had been removed

The new subset for image correlation is then

$$S_{New} = S - (S_{ref}^T U S_{def}^T)$$

where,

S_{ref}^I represents the set of points in crack region in reference image,

S_{def}^I represents the set of points in crack region in deformed image,

S is the subset of points.

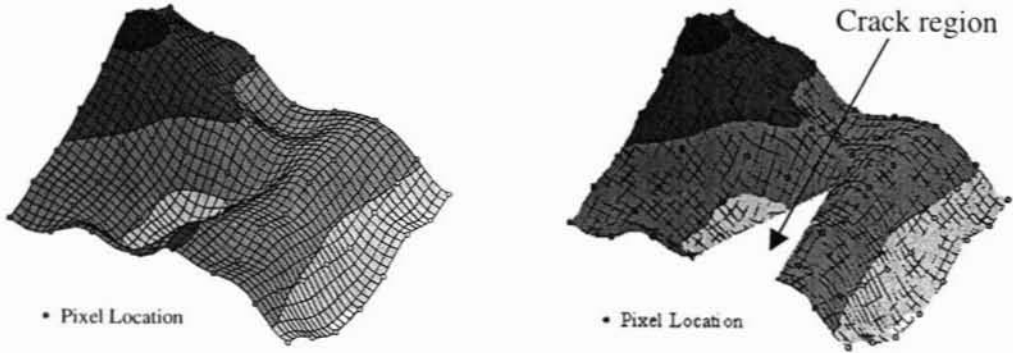


Figure 3.10: Bicubic Interpolation for modified correlation

The correlation coefficient is then given by

$$C = \frac{\sum_{S_p \in S_{New}} \{g(S_p) - h(S_p, S)\}^2}{\sum_{S_p \in S_{New}} g^2(S_p)}$$

Crack images generated by the connected component labeling method are used to find S_{New} at each iteration.

3.3.DeformedImagemaker Program

Deformed Imagemaker program is a Visual Basic program, which takes the deformed image as input and produces the reference image with the given input parameters. The input parameters are the displacement in the x direction, displacement in the y direction and the first order and second order gradients. It is tracking backwards from the deformed image to the reference image. The User's guide for this program is provided in Appendix G.

3.4.Results from New Algorithm

Theoretical images are used to validate the new algorithm to compute deformations near the crack region. A theoretical image of 512×486 pixels was generated using DeformedImagemaker program and used in the WinDIC program. Figure 3.9 shows the theoretical image used for validation of the new algorithm. The image shows the presence of a crack on the specimen. The input parameters for this image are

$$E = 200 \text{ Gpa}, K = 1.40 \text{ G pa} \cdot \sqrt{m} \text{ and } \nu = 0.3 .$$

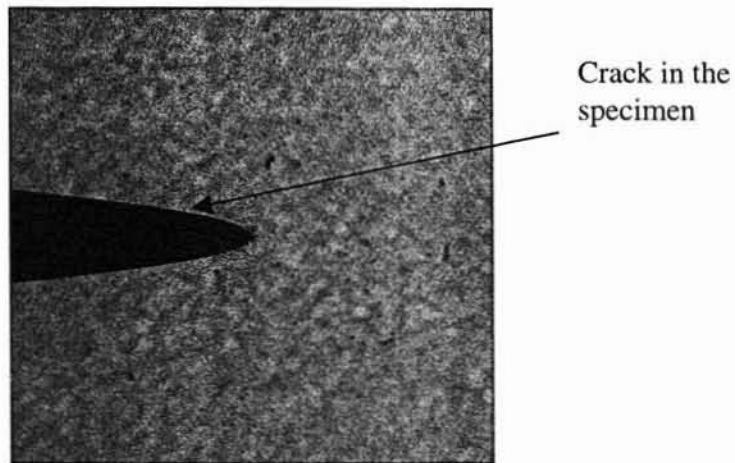


Figure 3.11: Theoretical image used for computation

Figure 3.10 shows the theoretical image with the nodal grid for computation. Figure 3.11 shows the theoretical image with the nodes that falls into the cracked region removed, after computation. Moreover the nodes that are near the edge of the crack have also converged. This serves as the validation for the algorithm to take the presence of crack in to account.

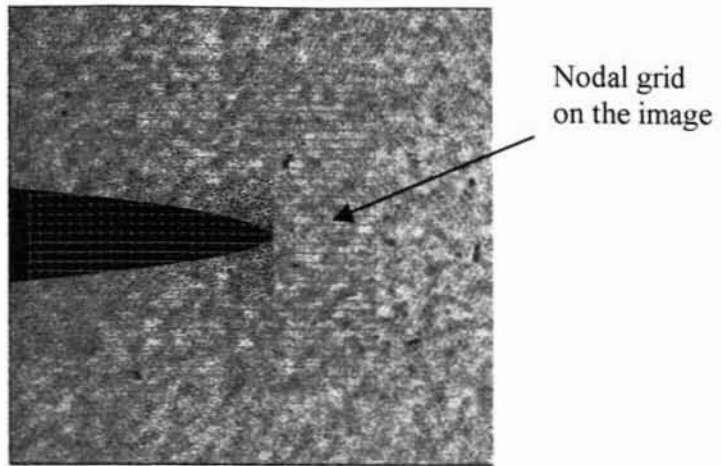


Figure 3.12: Theoretical image with nodal grid placed on it

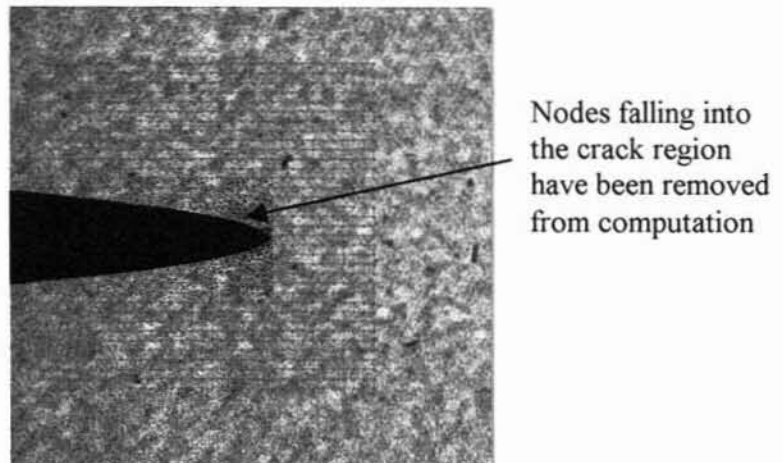


Figure 3.13: Theoretical image with nodes falling into the crack removed

CHAPTER 4

COMPUTATION OF J-INTEGRAL

4.1.J-integral

J-integral is a key parameter that has been developed to define the fracture conditions in a component experiencing both elastic and plastic deformation. A mathematical expression for the characterization of a line of the local stress-strain field around a crack front. The J -integral expression for a two-dimensional crack in the x - y plane with the crack front parallel to the y -axis is the line integral:

$$J = \int_{\Gamma} \left(W dy - T_i \frac{\partial u_i}{\partial x_1} ds \right)$$

where W is the strain energy density, s is the line coordinate, T is the traction vector and u is the displacement vector.

Figure 4.1 shows the crack and the path along which the J-integral is calculated. It is noted that J-integral is related to the energy in the vicinity of a crack in the presence of plastic deformation. Fracture of the specimen occurs when the J-integral reaches a critical value. The line S is the path along which the J-integral is to be computed. Then ds is a small segment of the path. n is the direction of the normal to the path. The frame along with the contour shows the coordinate system used with respect to the crack.

From figure 4.1 it can be seen that the path starts from the lower edge of the crack and ends on the upper edge. This is how the path should be chosen for J-integral computation.

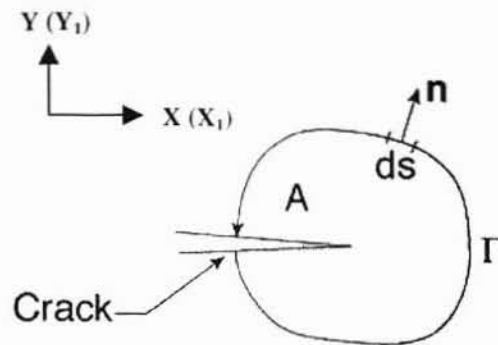


Figure 4.1: J-integral contour

J-integral is formulated for non linear elastic materials. Non linear elastic materials are similar to plastic materials during loading. Only restriction is that unloading is not permitted on these materials.

J-integral plays an important role in the assessment of fracture and fatigue performances of structures. It is used to measure the stress intensity factor around crack tips, which can be used to correlate the initiation of crack propagation. J-integral can be used to characterize the initiation of crack in a specimen.

Rice has shown that J-integral is path-independent. The strain energy determination using J at crack tip is valid as long as there is no unloading. J-integral cannot be defined under cyclic loading conditions also. As such J-integral has significance in terms of defining the stress and strain conditions for crack initiation under

monotonic loading conditions and also in presence of a limited amount of stable crack extension.

J is related to rate of change of potential energy with respect to change in crack size (Ashok Saxena., 1998). This interpretation is useful in showing that under linear elastic conditions, $J = g$, the Griffith's crack extension force. For either linear or non-linear elastic conditions, J is the energy made available at the crack tip per unit crack extension. The relation between J and K , the stress intensity factor is,

$$J = \frac{K^2}{E} \text{ for plane stress and}$$

$$J = \frac{K^2(1-\nu^2)}{E} \text{ for plane strain, where } \nu \text{ is the Poisson's ratio.}$$

J -integral uniquely characterizes the crack tip stress fields. As it is path independent, it can be measured at points remote from the crack tip. This property is very important when the calculations involve numerical solutions, as they are often not accurate in the immediate vicinity of the crack tip but increase in accuracy as one moves away from the crack tip.

4.2.Calculation of J-integral Around Crack Tips

The image correlation process gives the displacements in the corresponding directions namely U_x , U_y , V_x and V_y . The strains in the x , y and xy directions can be computed as

$$\epsilon_x = U_x$$

$$\epsilon_y = V_y$$

$$\varepsilon_{xy} = \frac{1}{2}(V_x + U_y)$$

(x_1, y_1) is the coordinate of the current node.

(x_2, y_2) is the coordinate of the next node.

The unit normals can be calculated by using the following forms.

Case 1: For outward normal to be on the right hand side

$$n_x = \frac{(y_1 - y_2)}{\sqrt{(x_2 - x_1)^2 + (y_2 - y_1)^2}}$$

$$n_y = \frac{(x_1 - x_2)}{\sqrt{(x_2 - x_1)^2 + (y_2 - y_1)^2}}$$

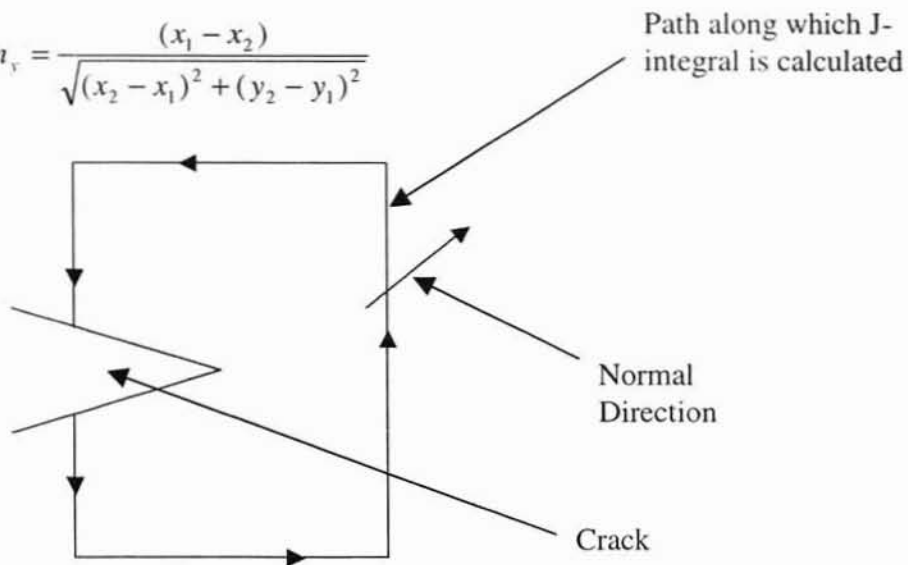


Figure 4.2: Direction of right outward normal

Case 2: For outward normal to be on the left hand side

$$n_x = \frac{(y_2 - y_1)}{\sqrt{(x_2 - x_1)^2 + (y_2 - y_1)^2}}$$

$$n_y = \frac{(x_2 - x_1)}{\sqrt{(x_2 - x_1)^2 + (y_2 - y_1)^2}}$$

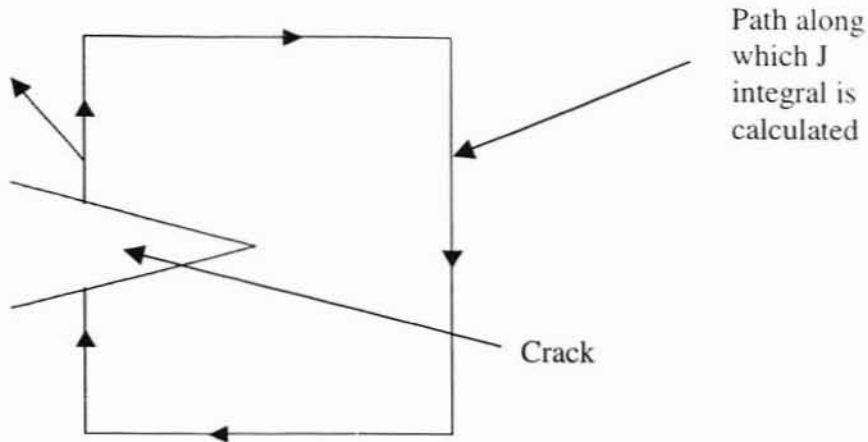


Figure 4.3: Direction of left outward normal

The traction components are in the following form:

$$T_i = \sigma_{ij} n_j$$

then

$$T_x = \sigma_{xx} n_x + \sigma_{xy} n_y$$

$$T_y = \sigma_{yy} n_y + \sigma_{xy} n_x$$

As can be seen from the formula for traction components, the stress components need to be calculated. The computations of stress components from strains are described for several materials as follows.

From the values of traction and stress the J-integral can be calculated along the path. The area under the stress-strain curve can be used as the rough verification for the J-integral value obtained.

4.3.Theories Used for the Calculation of Stress

In this part, the computations of stress components are described, these stress components are used in calculating stress. J-integral was calculated using the above form based on three theories for calculating stress. The three theories used were:

4.3.1. Linear Elastic Model

The equation for calculating the stress components using linear elastic model is

$$\sigma_{ij} = \lambda \varepsilon_{kk} \delta_{ij} + 2\mu \varepsilon_{ij},$$

where λ is the Lamé's constant, it can be computed in terms of Young's Modulus E and Poisson's ratio ν , ε_{ij} are the components of strain, δ_{ij} is the Kronecker Delta.

$$\lambda = \frac{\nu E}{(1 + \nu)(1 - 2\nu)}$$

where μ is the shear modulus, it can be computed by $\mu = \frac{E}{2(1 + \nu)}$.

4.3.2. Ramberg-Osgood Model

This model can be used for materials that show a non linear behavior when the material is under deformation.

The power law relation for this model in one dimensional stress state is given by

$$\varepsilon = \frac{\sigma}{E}, \sigma < \sigma_0,$$

$$\varepsilon = \frac{\sigma}{E} + \frac{\alpha \sigma_0}{E} \left(\frac{\sigma}{\sigma_0} \right)^n, \sigma \geq \sigma_0.$$

where, ε is the strain, σ is the stress in psi, α is the hardening coefficient, n is the non-linearity index, E is the Young's modulus of the material and σ_0 is the yield stress.

$$\varepsilon_z = -\varepsilon_x - \varepsilon_y.$$

$$S_0 = E\varepsilon_0, \text{ where } \varepsilon_0 \text{ is the yield strain.}$$

$$S_1 = 0$$

$$S_2 = S_0$$

$$\text{Let } P = \sqrt{\frac{2}{3}(\varepsilon_x^2 + \varepsilon_y^2 + \varepsilon_z^2 + 2\varepsilon_{xy}^2)},$$

$$e3 = P,$$

$$ec = -100,$$

Steps 1 to 4 are carried out till $((ec - P) / ec)$ reaches a value less than tolerance (0.000000001).

$$1) \ e1 = \varepsilon_0 \cdot \left(\frac{S_1}{S_0} + \alpha \left(\frac{S_1}{S_0} \right)^N \right)$$

$$2) \ e2 = \varepsilon_0 \cdot \left(\frac{S_2}{S_0} + \alpha \left(\frac{S_2}{S_0} \right)^N \right)$$

$$3) \ S_3 = S_1 + \frac{(S_2 - S_1)}{(e2 - e1)} \cdot (e3 - e1)$$

$$4) \ ec = \varepsilon_0 \cdot \left(\frac{S_3}{S_0} + \alpha \cdot \left(\frac{S_3}{S_0} \right)^N \right)$$

$$S_1 = S_2$$

$$S_2 = S_3$$

$$\text{Let } es = \frac{S_2}{P},$$

$$\text{Let } A = \frac{1}{es},$$

$$B = \frac{\nu}{E} + \frac{1}{2} \left(\frac{1}{es} - \frac{1}{E} \right),$$

$$C = \frac{(1+\nu)}{E} + \frac{3}{2} \left(\frac{1}{es} - \frac{1}{E} \right),$$

$$F = A^2 - B^2.$$

Then the components of stress are given by,

$$\sigma_{11} = \frac{1}{F}(A\varepsilon_x + B\varepsilon_y)$$

$$\sigma_{22} = \frac{1}{F}(B\varepsilon_x + A\varepsilon_y)$$

$$\sigma_{12} = \frac{\varepsilon_{xy}}{C}$$

Thus the components of stress are evaluated from strains using the Ramberg-Osgood model. The validation of this algorithm alone is also carried out separately. The strain values are given as input and stresses are calculated. Then the reverse calculation is done to get the strain values.

4.3.3. Bilinear Model

The governing equation for a bilinear material is given by,

$$\varepsilon_{ij} = \frac{1}{E}[(1+\nu)\sigma_{ij} - \nu\delta_{ij}\sigma_{mn}] \text{ when } \sigma_e < \sigma_y$$

$$\varepsilon_{ij} = \frac{1}{E} \left[(1+\nu)\sigma_{ij} - \nu\delta_{ij}\sigma_{mn} + \frac{3}{2}(\alpha^{-1} - 1) \frac{\sigma_e - \sigma_y}{\sigma_e} S_{ij} \right] \text{ when } \sigma_e > \sigma_y$$

where

ν is the Poisson's ratio, $\alpha = E_s/E$, E_s is the secant modulus, δ_{ij} is the Kronecker

delta, S_{ij} are the deviatoric stress components defined by,

$$S_{ij} = \sigma_{ij} - \frac{1}{3}\sigma_{nn}\delta_{ij}$$

$$\sigma_e = \sqrt{\left(\frac{3}{2}S_{ij}S_{ij}\right)}$$

The stress at the crack tip reaches infinity. So the value of $\frac{\sigma_e - \sigma_y}{\sigma_e}$ approached unity.

Based on the assumption the equation reduces to

$$\varepsilon_{ij} = \frac{1}{E} \left[(1+\nu)\sigma_{ij} - \nu\delta_{ij}\sigma_{mn} + \frac{3}{2}(\alpha^{-1} - 1)S_{ij} \right]$$

The method for obtaining stress values from strains is explained with respect to bilinear model. The following are the steps involved in arriving at the final equation for stress,

Let $i = j = 1$, which yields,

$$S_{11} = \sigma_{11} - \frac{1}{3}(\sigma_{11} + \sigma_{22} + \sigma_{33})$$

Therefore,

$$S_{11} = \frac{2}{3}\sigma_{11} - \frac{1}{3}\sigma_{22} - \frac{1}{3}\sigma_{33}$$

$$\varepsilon_{11} = \frac{1}{E} \left[(1+\nu)\sigma_{11} - \nu(\sigma_{11} + \sigma_{22} + \sigma_{33}) + \frac{3}{2} \left(\frac{E}{E_s} - 1 \right) S_{11} \right]$$

$$\varepsilon_{11} = \frac{1}{E} \left[(1+\nu)\sigma_{11} - \nu(\sigma_{11} + \sigma_{22} + \sigma_{33}) + \frac{3}{2} \left(\frac{E}{E_s} - 1 \right) \left(\frac{2}{3}\sigma_{11} - \frac{1}{3}\sigma_{22} - \frac{1}{3}\sigma_{33} \right) \right]$$

let $P = \frac{E}{E_s} - 1$

$$\varepsilon_{11} = \frac{1}{E} \left[\sigma_{11} - \nu\sigma_{22} - \nu\sigma_{33} + P \left(\sigma_{11} - \frac{1}{2}\sigma_{22} - \frac{1}{2}\sigma_{33} \right) \right]$$

Therefore,

$$\varepsilon_{11} = \frac{1}{E} \left[\sigma_{11}(1+P) - \sigma_{22} \left(\nu - \frac{P}{2} \right) - \sigma_{33} \left(\nu - \frac{P}{2} \right) \right]$$

Similarly for $i = j = 2$

$$\varepsilon_{22} = \frac{1}{E} \left[\sigma_{22}(1+P) - \sigma_{11} \left(\nu - \frac{P}{2} \right) - \sigma_{33} \left(\nu - \frac{P}{2} \right) \right]$$

and when $i = j = 3$

$$\varepsilon_{33} = \frac{1}{E} \left[\sigma_{33}(1+P) - \sigma_{11} \left(\nu - \frac{P}{2} \right) - \sigma_{22} \left(\nu - \frac{P}{2} \right) \right]$$

Let $D = \nu - \frac{P}{2}$

$$\varepsilon_{11} = \frac{1}{E} [\sigma_{11}(1+P) - D\sigma_{22} - D\sigma_{33}]$$

$$\varepsilon_{22} = \frac{1}{E} [\sigma_{22}(1+P) - D\sigma_{11} - D\sigma_{33}]$$

$$\varepsilon_{33} = \frac{1}{E} [\sigma_{33}(1+P) - D\sigma_{11} - D\sigma_{22}]$$

when the above set of equations are written in matrix form we get,

$$\begin{bmatrix} \varepsilon_{11} \\ \varepsilon_{22} \\ \varepsilon_{33} \end{bmatrix} = \frac{1}{E} \begin{bmatrix} (1+P) & -D & -D \\ -D & (1+P) & -D \\ -D & -D & (1+P) \end{bmatrix} \begin{bmatrix} \sigma_{11} \\ \sigma_{22} \\ \sigma_{33} \end{bmatrix}$$

The symbolic form of the above equation is given by,

$$[\varepsilon] = \frac{1}{E} [M] [\sigma]$$

From this the stress matrix can be found using the following relation,

$$[\sigma] = E[\varepsilon][M]^{-1}$$

4.4 Validation of J integral Algorithm using Ideal Images

Ideal images were generated using Deformed image maker with the following input parameters:

$$\text{Stress intensity factor } K = 1.40 \text{ G pa} \cdot \sqrt{m} ,$$

$$\text{Poisson's ratio} = 0.3,$$

$$\text{Young's Modulus } E = 200 \text{ G pa}.$$

With the above values for parameters a displacement field was prescribed to the images using DeformedImagemaker program. The theoretical displacement fields is given by the asymptotic displacement field in mode I crack problem.

$$U = \frac{K}{2E} \sqrt{\frac{r}{2\pi}} (1 + \nu) \left[(2\kappa - 1) \cos\left(\frac{\theta}{2}\right) - \cos\left(\frac{3\theta}{2}\right) \right],$$

$$V = \frac{K}{2E} \sqrt{\frac{r}{2\pi}} (1 + \nu) \left[(2\kappa + 1) \sin\left(\frac{\theta}{2}\right) - \sin\left(\frac{3\theta}{2}\right) \right],$$

where, U is the displacement in the x direction and V is the displacement in the y direction, (r, θ) is the position with respect to the crack tip, K is the stress intensity factor,

$\kappa = 3 - 4\nu$ for plane strain, $\kappa = \frac{3 - \nu}{1 + \nu}$ for plane stress, ν is the Poisson's ratio, in this case

plane strain condition is considered, E is the Young's modulus.

Figure 4.2 shows the reference image that was generated using the deformed image, which is shown in Figure 4.3. The J integral was calculated using the constitutive law of the linear elastic material. The results are shown in Table 1. The fracture toughness of a material and the J integral are related by the following equation

$$J = \frac{K^2}{E}$$

The K values for the theoretical images were calculated from the above-mentioned equation. The ideal images actually does not show the presence of a crack, but when the images are examined it can be found that reference image looks like it has been shrunk by holding the specimen along its edges, and the deformed image looks like it has been expanded, thus accounting for the crack. The prescribed value of K , the stress intensity factor is $1.4 \text{ Gpa} \cdot \sqrt{\text{m}}$.

Table 4.1 shows the results that were obtained for the theoretical images with WinDIC. The results show that the prescribed fracture toughness (K) values are recovered. The maximum error is 12.40%, which suggests that the J integral algorithm is validated using ideal images. The first path is the path that is close to the crack tip, where the J integral values obtained is not very accurate. As the path move outwards the error involved in the recovery of K is reducing and it remains almost a constant.

Table 4.1: Results for theoretical images

Path	J integral ($pa \cdot m$)	K ($pa \cdot \sqrt{m}$)	Error in K (%)
1	7519639.061	1226347346	12.403
2	8445931.041	1299686965	7.165
3	8962927.645	1338874725	4.366
4	8921503.58	1335777196	4.587
5	8906648.316	1334664626	4.666
6	8852798.987	1330623838	4.955
7	8811407.305	1327509496	5.177
8	8757930.825	1323475034	5.466
9	8708797.780	1319757385	5.731
10	8670696.449	1316867226	5.938
11	8607571.163	1312064874	6.281
12	8874825.444	1332278157	4.837
13	8523293.326	1305625775	6.741

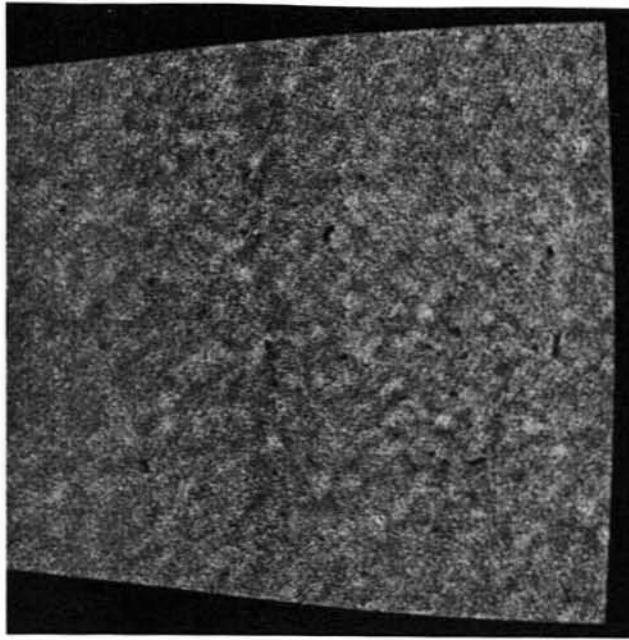


Figure 4.4: Reference ideal image

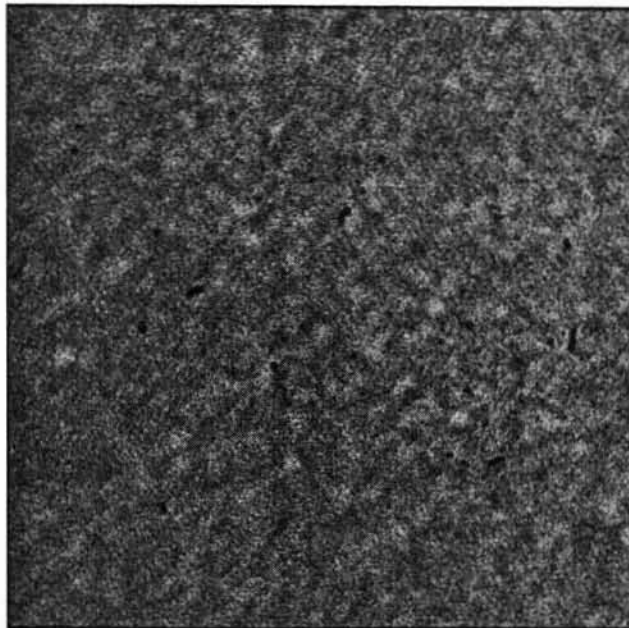


Figure 4.5: Deformed Ideal image

4.5. J integral for Actual Specimens

4.5.1. Uniaxial Tensile Test on Rubbery Particulate Composite

Images were obtained from tests performed on actual specimens with cracks. The materials for these specimens were rubbery particulate composites. The test conducted on the specimens is the uniaxial tension test. The images obtained were transformed into uncompressed 8-bit grayscale images for using in WinDIC. The images used for the test are shown in the APPENDIX C. The tests results obtained from this test are shown in table 4.2. The results for the last 4 images are shown in the Table 4.2. The material properties are, $E = 4741KPa$, $\nu = 0.499$, $\epsilon_0 = 0.092$.

Table 4.2: J integral ($KPa \cdot m$) values for uniaxial tensile test on particulate composite.

Distance (m)	04.tif	05.tif	06.tif	07.tif	08.tif	09.tif	10.tif	12.tif
0.030	0.216	0.404	0.183	1.655	0.662	2.105	1.802	2.500
0.038	0.237	0.476	0.898	1.934	1.715	2.357	2.268	2.698
0.046	0.246	0.571	1.028	1.684	2.029	2.499	2.295	2.942
0.053	0.231	0.491	1.061	1.842	2.069	2.527	2.595	3.122
0.061	0.255	0.493	1.077	1.895	2.016	2.619	2.549	3.308
0.068	0.270	0.541	1.119	1.867	2.149	2.543	2.611	3.191
0.076	0.287	0.610	1.144	1.778	2.163	2.621	2.716	3.332
0.084	0.292	0.539	1.180	1.883	2.300	2.644	2.904	3.440
0.091	0.292	0.607	1.184	1.952	2.273	2.719	2.898	3.468

Then K values for the specimen is calculated using the J integral values that were obtained from the WinDIC test. Table 4.3 shows the K values for different images.

The values suggest that the variation in K values for a particular image is less, which suggests that the J integral is path independent. Thus the path independent property of J integral is verified. Moreover the critical value for K occurs at the time of propagation of the crack in the specimen, which in the present case occurs from image 5 to 6.

The critical value of K was found to be $64KPa \cdot \sqrt{m}$ from the force at the time when the crack initiates during the test. The values of K for image 5(K-5) and image 6(K-6) suggest that the average of the K lies in the required value region. Thus the K values have been recovered and at the same time the J -integral values are constant which suggests that the algorithm is validated. Due to the inhomogeneity of the particulate composite material a variation of 20% is allowed in the value of J -integral.

Table 4.3: Stress intensity factor ($KPa \cdot \sqrt{m}$) for uniaxial tensile test on particulate composite.

Distance								
(m)	K-4	K-5	K-6	K-7	K-8	K-9	K-10	K-12
0.030	31.967	43.781	29.453	88.566	56.009	99.890	92.432	108.854
0.038	33.526	47.492	65.226	95.754	90.159	105.693	103.687	113.095
0.046	34.139	52.005	69.812	89.354	98.066	108.827	104.305	118.083
0.053	33.065	48.263	70.921	93.446	99.022	109.451	110.905	121.643
0.061	34.766	48.340	71.445	94.778	97.757	111.421	109.917	125.224
0.068	35.789	50.622	72.838	94.083	100.916	109.788	111.256	122.990
0.076	36.897	53.756	73.637	91.797	101.261	111.454	113.473	125.681
0.084	37.200	50.548	74.772	94.475	104.409	111.959	117.325	127.686
0.091	37.200	53.640	74.911	96.190	103.791	113.524	117.208	128.218

Figure 4.6 shows the plot of fracture toughness versus path number for different images in test 10. The plot shows that the variation of fracture toughness for different images after initial paths is less. The initial paths are the paths that are very close to the crack tip where the J integral calculations are not so accurate because of some unconverged node near the crack tip.

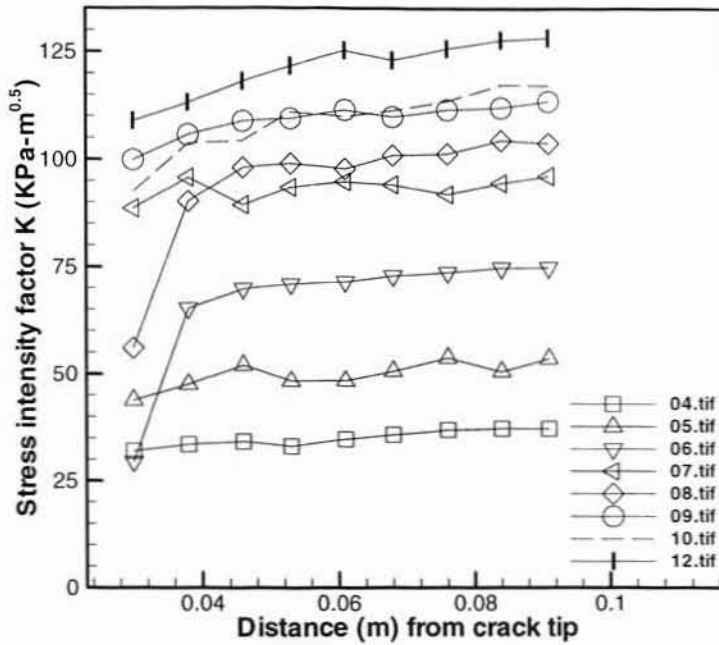


Figure 4.6: Plot of K Vs Distance for uniaxial tensile test on particulate composite.

4.5.2. Test Results from Materials Obeying Bilinear Model

4.5.2.1. Particulate Composite Specimen Tested at 20% Pre-strain

Images from tests carried out on bilinear materials are used in WinDIC for obtaining results based on bilinear model. Figure 4.7 shows the stress-strain curve for uniaxial tension test with 20% pre-strain, which obeys bilinear model. The dashed line shows the actual curve. The first linear region has a modulus of 2034 KPa. The second region's modulus led the secant modulus (E_s) is 1330 KPa. These values are supplied to the WinDIC program with the help of the user interface.

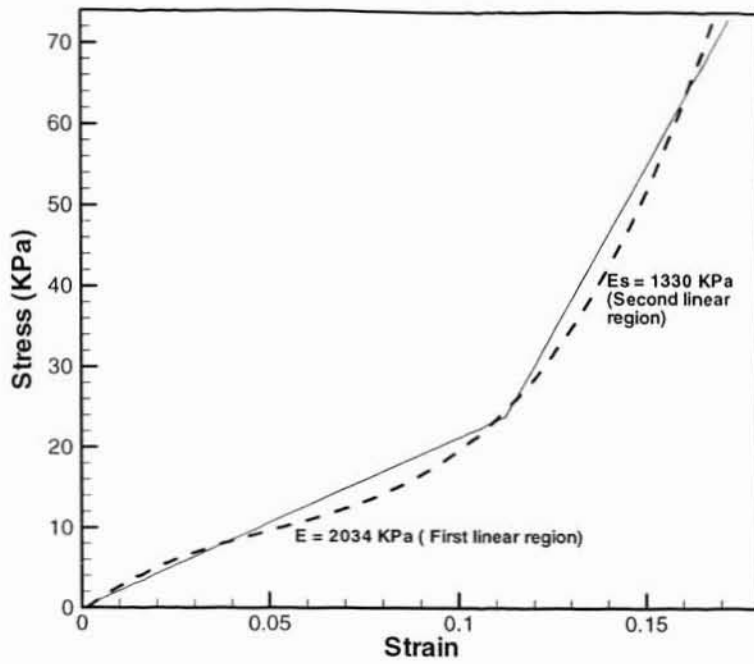


Figure 4.7: Stress-strain curve for 20% pre-strain test
 Table 4.4: J-integral (KPa-m) values for 20% pre-strain test

Distance (m)	10	11	12	13	14
0.030	0.018	0.098	0.300	0.342	0.440
0.038	0.025	0.172	0.368	0.413	0.495
0.046	0.033	0.239	0.455	0.557	0.495
0.053	0.038	0.233	0.427	0.539	0.556
0.061	0.044	0.257	0.467	0.591	0.616
0.068	0.037	0.228	0.424	0.546	0.614
0.076	0.036	0.258	0.439	0.553	0.627
0.084	0.037	0.277	0.460	0.554	0.616
0.091	0.040	0.293	0.482	0.580	0.646

The J-integral values obtained from WinDIC for 20% pre-strain test is shown in Table 4.4. The images, which were used in this computation, are shown in APPENDIX D. The crack propagation in this test starts on image 12.tif. The J-integral value obtained on this image serves as the critical value of J.

4.5.2.2. Particulate Composite Specimen Tested at 15% Pre-strain

Next images from another set of images of material obeying bilinear model were used to compute J-integral values. The stress strain curve for second set of material obeying bilinear model is shown in figure 4.8. The modulus for the first linear region is 1889 KPa and that of the second linear region is 1510 KPa. Table 4 shows the J-integral values obtained from WinDIC on 15% pre-strain test images. The images, which were used in this computation, are shown in APPENDIX E. The crack propagation for this test starts on image 14.tif. The J-integral obtained for this image serves as the critical value of J for this test.

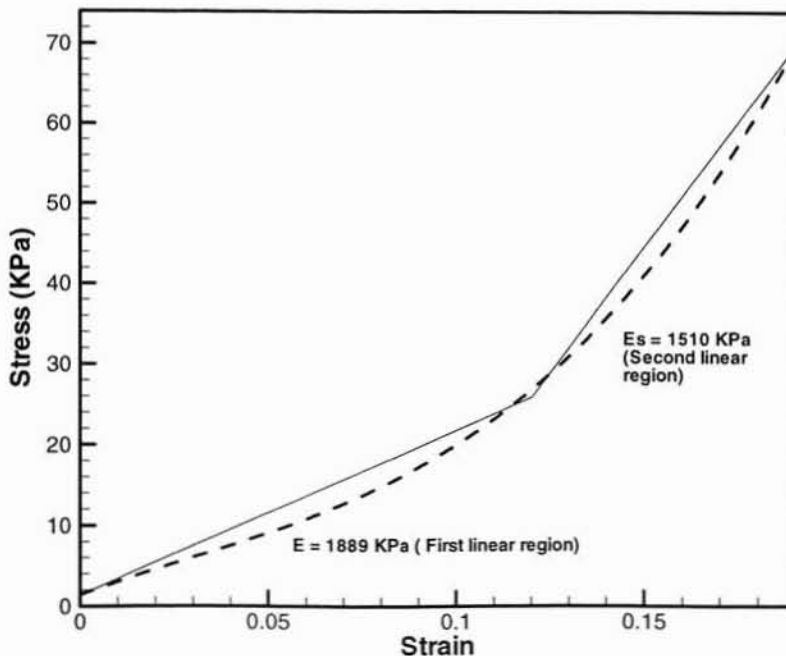


Figure 4.8: Stress-strain curve for 15% pre-strain test

Table 4.5: J-integral (KPa-m) values for 15% pre-strain test

Distance (m)	12	14	15	16	17	18
0.030	0.054	0.201	0.308	-0.368	1.243	0.928
0.038	0.099	0.356	0.629	0.872	0.912	0.974
0.046	0.130	0.374	0.664	0.904	0.866	0.927
0.053	0.146	0.418	0.720	0.910	0.951	1.056
0.061	0.154	0.433	0.771	0.947	1.049	1.117
0.068	0.168	0.469	0.816	1.003	1.100	1.153
0.076	0.196	0.498	0.859	1.041	1.156	1.213

CHAPTER 5

VALIDATION OF ALGORITHM USING NANOCOMPOSITE SPECIMENS

The improved algorithm for measuring deformation near a crack tip is evaluated using test performed on bending specimens. The material chosen for the test is epoxy nanocomposite. A series of three-point bending tests were conducted on nanocomposite specimens. The deformation fields were observed and convergent results of deformations were obtained near crack tips. The nodes falling in to the crack region have also been removed from deformation computation. Thus a validation of the improvements to DIC was carried out using nanocomposite specimens.

5.1. Background on Nanocomposites

Nanocomposites are an emerging class of mineral-filled plastics that contain relatively small amounts ($\leq 10\%$) of nanometer-sized clay particles. The definition of nanocomposite material has broadened significantly to encompass a large variety of systems such as one-dimensional, two-dimensional, three-dimensional and amorphous materials, made of distinctly dissimilar components and mixed at the nanometer scale.

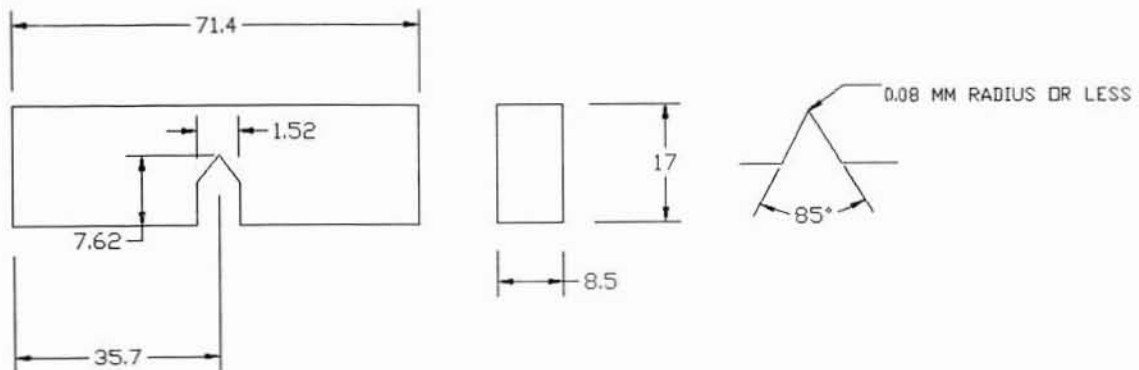
The class of nanocomposite materials is a fast growing area of research. Significant effort is focused on the ability to obtain control of the nanoscale structures via innovative synthetic approaches. The properties of nanocomposite materials depend on both the properties of their individual components and also on their morphology and interfacial characteristics.

5.2. Specimen Preparation

The epoxy resin Epon-82, a bisphenol-A derivative made by Shell, is first heated to 60°C to lower the viscosity, since lower viscosity promotes enhanced dispersion. The nanoclay particles (MMT) are then hand mixed together with the resin for about 20 minutes. Adding a few drops of the mixture onto a glass laboratory slide and pressing it together with another slide check dispersion of the nanoclay. A light source is used against those slides to check for solid particles. If the slides are found to be a clear mixture then the dispersion is complete.

When the epoxy-nanoclay mixture is ready, curing agent and accelerator are added into the resin. Once this mixture has been thoroughly mixed, the mixture is then degassed and cured on a mold accordingly. Thus the nanocomposite specimens are prepared.

The prepared materials are then machined into standard three-point bending specimen. The specimen geometry is shown in Figure 5.1. ASTM E-399 was used to design the sample. The basic dimension, namely the width is taken to be 17mm.



All dimensions are in millimeters

Figure 5.1: Specimen dimensions.

Samples were machined and sharp cracks were introduced for each specimen by a new razor blade. Annealing is carried out to relieve the residual stresses present in the

specimen due to machining and various processes carried out on the specimen. The glass transition temperature of the epoxy nanocomposites is 130°C. The specimens were annealed at 125°C. Specimens were pre-heated to a temperature of 100°C before being subjected to a temperature of 125°C. The specimens were maintained at 125°C for 4 hours so that structural rearrangements can take place. Then the temperature was brought to room temperature. After annealing the specimens were held in dessicator at $50 \pm 2\%$ relative humidity level for a period of 3 days. All specimens had approximately the same aging times prior to testing.

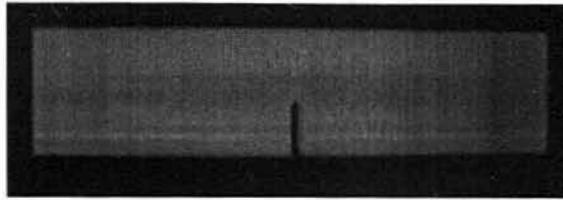


Figure 5.2: Three-point bending specimen.

5.3.Experimental Setup

The loading setup is shown in Figure 5.3. An MTS three-point bend fixture is placed on the Instron machine. Care is taken to see that the fixture is placed in a rigid manner to prevent any shaking of the fixture, to avoid inaccurate results.

In this test the cross-head moves down as the load is to be applied on the specimen. The magnitude of compressive force range is set from 0 N to 1120 N as the specimen can break between these loads. The cross-head speed is set to 2 mm/min. The cross-head moves downwards until the specimen breaks. The center-to-center span between the supporting rollers is set to 68mm according to ASTM standards

LabView is used for capturing the data from the Instron machine. Data such as load and extension are read from the machine. The time interval between each data acquisition

can be controlled using the provisions in the software. The Data Acquisition (DAQ) board has provisions for capturing the data from the machine to the computer.

Before the data was acquired the load cell was calibrated with DAQ using dead-weight to facilitate in getting the correct data from the Instron machine to the computer. The calibration can be used to update the equation in the .vi diagram in the LabView file. The data such as load applied to the specimen and the displacement of the specimen can be acquired from the LabView software.

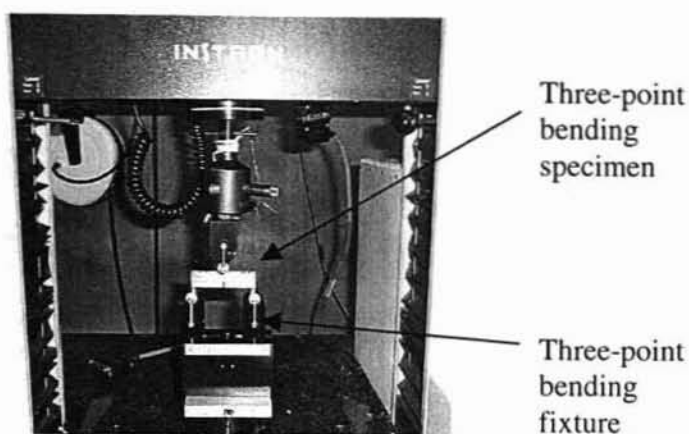


Figure 5.3: Instron machine setup.

The data acquisition setup is made ready before the cross-head of the Instron machine is moved down. Image acquisition intervals are set and the LabView data acquisition is also made ready. As the cross-head moves down the images are acquired until the specimen breaks. The load at which the specimen breaks is obtained from the data file generated by the LabView software. The length of the crack is measured from the fractured surface after the test to get accurate value of the length of the crack. The experiments were repeated for epoxy nanocomposite specimens with different set of loading of nanoclay particles.

5.4. Experimental Procedures

The reference and the deformed image used in the calculation of J-integral are shown in figures 5.4 and 5.5 respectively. The reference image has the reference nodal grid on it. Figure 5.5 shows that the nodes that fall into the crack region have been removed. Most of the nodes surrounding the crack have all converged to give results of strain near the crack edge.

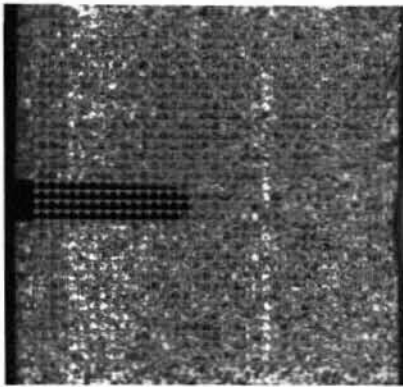


Figure 5.4: Reference image.

Nodes falling into the crack region have been removed

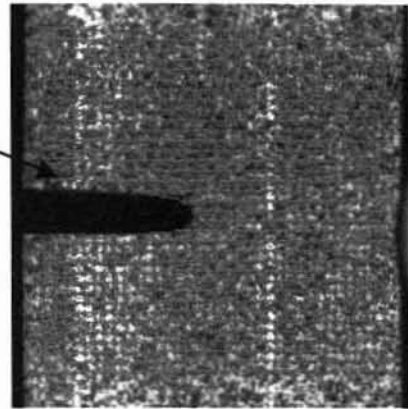


Figure 5.5: Deformed image.

Digital image correlation is used to find the strain energy rates (G_{IC}) and compare the values with the fracture toughness value obtained from the fracture toughness tests.

$$G_{IC} = \frac{K_{IC}^2}{E}$$

where K_{IC} is the fracture toughness and E is the young's modulus.

5.5. Results and Discussion

The fracture toughness of the three-point bending specimen is determined using the relation by Lee and Yee (2000),

$$K_{IC} = Y \frac{3PS\sqrt{a}}{2BW^2}$$

$$Y = 1.93 - 3.07(a/W) + 14.52(a/W)^2 - 25.11(a/W)^3 + 25.80(a/W)^4$$

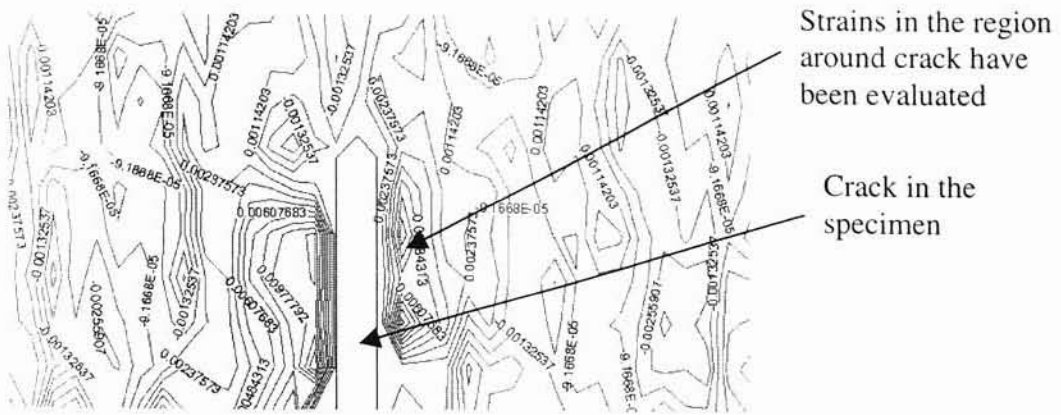
where Y is the shape factor, P is the load at failure. S is the length of the span (68 mm), a is the crack length and W is the width of the specimen (17 mm).

Table 5.1: Fracture Toughness Values of samples

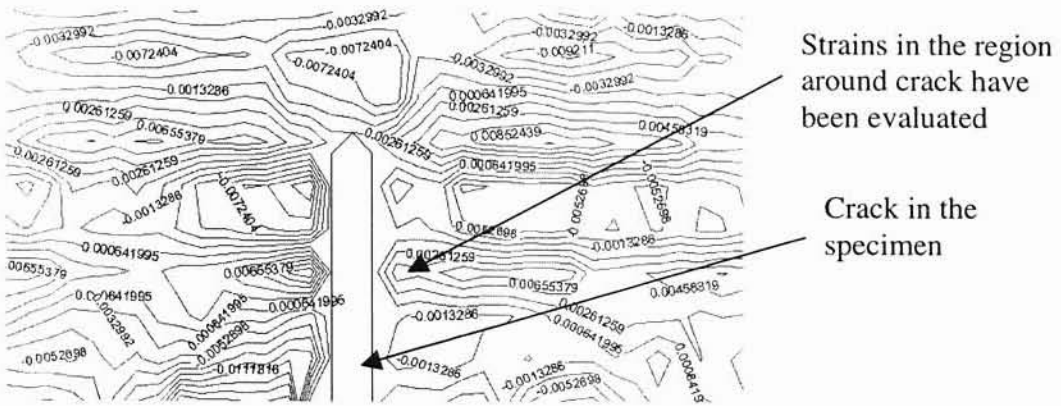
Nanoclay loading in Nanocomposites (%)	Fracture Toughness ($MPa \cdot \sqrt{m}$)
0	2.52
3	1.53
5	1.39
7	0.90

Table 5.1 shows the fracture toughness for nanocomposites with different nanoclay loadings between 0% and 7%. The fracture toughness values are seen to be decreasing with the increase in the percentage of the nanoclay particles in the epoxy resin. The brittleness of the specimen appears to increase with the increase in the addition of nanoclay particles to the neat resin.

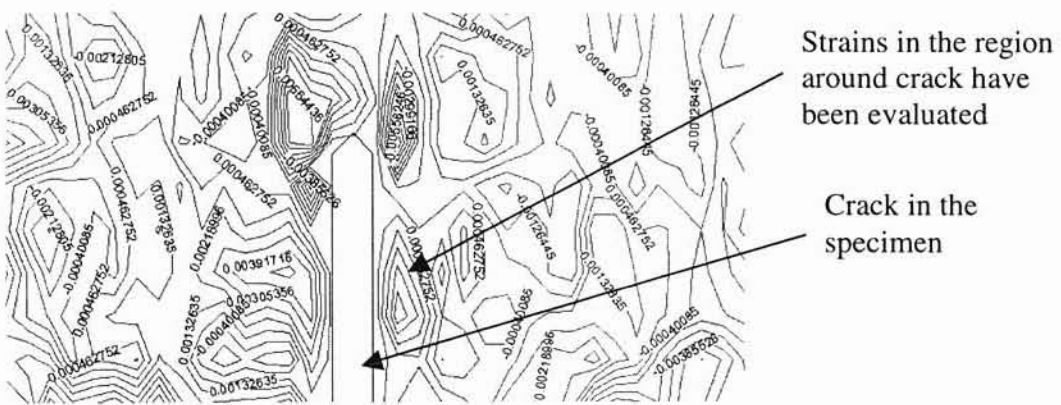
Figure 5.6(a) shows the distribution of strains in the X direction. The strains were plotted using Tecplot 9.0. The contours show the distribution of strain along the specimen near the crack region. These strain values were obtained from each node on the nodal grid to be plotted by Tecplot. From the figure it can be seen that the strain values very near to the crack can be evaluated with the present algorithm. Thus it can be seen that the nodes falling into the crack region have been removed from computation. The strain values are very low as the images acquired were well before crack propagation in the specimen. The crack origination and breakage of the specimen takes place within a fraction of a second. As the specimens were very brittle, crack propagation cannot be seen on the images.



(a) ϵ_{xx}



(b) ϵ_{yy}



(c) ϵ_{xy}

Figure 5.6: Strain Distributions for Nanocomposite specimen with 3% nanoclay loading.

Figure 5.6 shows the contour plot for the strains in the specimen during the test. The strain values are not symmetric about the crack region.

CHAPTER 6

CONCLUSIONS

1. An improved algorithm for taking the cracks into account is proposed and validated. The algorithm can take the presence of crack into account for computing the deformations in the specimen. The validation was carried out using ideal images generated with the Deformed Image maker program. This shows that the WinDIC can be used to take any type of cracks into account. As the crack could be detected on the specimen the deformation values near the crack edges can also be detected. Thus the DIC can be used to obtain deformation values near a crack, which was not possible with the old algorithm.

2. The nodes that fall into the crack region are removed from computation, and are not taken into account for calculation of deformation. In the previous algorithm there was no provision for removing the nodes that fall into the crack region, from deformation computation. This problem has been overcome with the present algorithm.

3. A method for computing J-integral using DIC is proposed and validated. The property of path independence of J-integral can be seen from the results obtained for the test shown. The results obtained for the tests are almost constant with very little variation. This variation can be attributed to the numerical algorithms that are used in the computations.

REFERENCES

- Bezerra, L., and Medeiros, J.M.S., "Using boundary elements and J-integral for the determination of K_I in fracture mechanics," IABEM (2002).
- Bouchard, P.J., Goldthorpe, M.R., and Prottey, P., "J-integral and local damage fracture analyses for a pump casing containing large weld repairs," *International Journal of Pressure Vessels and Piping*, 78, 295-305 (2001).
- Bruck, H.A., McNeil, S.R., Sutton, M.A., and Peters, W.H., "Digital Image Correlation using Newton-Raphson method of partial differential correction," *Experimental Mechanics*, 29 (3), 261-267 (1989).
- Chevalier, L., Calloch, S., Hild, F., and Marco, Y., "Digital Image Correlation used to analyze the multiaxial behavior of rubber-like materials," *Eur. J. Mech. A*, 20, 169-187 (2001).
- George.E.Dieter., "Mechanical Metallurgy", 3rd Edition, McGrawHill Inc (1986).
- Gerald, C. F., and Wheatley, P. O., "Applied Numerical Analysis", Addison-Wesley Publishing Company, Reading, Massachusetts, (1994).
- Hussain, M., Nakahira, A., Nishijima, S., and Niihara, K., "Fracture behavior and fracture toughness of particulate filled epoxy composites," *Materials Letters* 27., 21-25 (1996).
- Haddi, A., and Weichert, D., "On the computation of the J-integral for three-dimensional geometries in inhomogeneous materials," *Computational Materials Science*, 5, 143-150, (1996).
- Kim, Y.J., Shim, D.J., Choi, J.B., and Kim, Y.J., "Approximate J estimates for tension-loaded plates with semi-elliptical surface cracks," *Engineering Fracture Mechanics*, 69, 1447-1463 (2002).
- Kim, Y.J., "Experimental J estimation equations for single-edge-cracked bars in four-point bend: homogeneous and bi-material specimens," *Engineering Fracture Mechanics*, 69, 793-811 (2002).
- Knauss, W.G., Gonzalez, J., "Strain inhomogeneity and discontinuous crack growth in a particulate composite", *Journal of Mechanics and Physics of Solids*, 46(10), 1981-1995 (1998).

Lee, J., and Yee, A.F., "Role of inherent matrix toughness on fracture of glass bead filled epoxies", *Polymer* 41, 8375-8385 (2000).

Lu, H., Cary, P.D., "Deformation measurements by Digital Image Correlation: implementation of second-order displacement gradient", *Experimental Mechanics*, 4(4), 393-310 (2000).

Lu, H., Ganesan Balaji., and S.Hariharan., "Deformation measurements by Digital Image Correlation: implementation of third order displacement gradient", *Creative Component report*, (2000).

McNeill, S.R., Peters, W.H., and Sutton, M.A., "Estimation of stress intensity factor by Digital Image Correlation," *Engineering Fracture Mechanics*, 101-112 (1987).

Peters, W.H., and Ranson, W.F., "Digital imaging techniques in experimental stress analysis," *Opt. Eng.*, 21 (3), 427-432 (1982).

Rahman, S., "Probabilistic fracture mechanics: J-estimation and finite element methods," *Engineering Fracture Mechanics*, 68, 107-125 (2001).

Saxena, A., "Non linear fracture mechanics for engineers", CRC Press LLC (1998).

Sun, Z., Lyons, J.S., and McNeill, S.R., "Measuring microscopic deformations with digital image correlation," *Optics and Lasers in Engineering*, 27, 409-428 (1997).

Sutton, M.A., Wolaters, W.J., Peters, W.H., Ranson, W.F., and McNeill, S.R., "Determination of displacements using an improved digital image correlation method," *Image Vision Computing*, 1 (3), 133-139 (1983).

Sutton, M.A., Turner, J.L., Bruck, H.A., and Chae, T.A., "Full-field representation of discretely sampled surface deformation for displacement and strain analysis", *Experimental Mechanics*, 31(2), (168-177) (1991).

Sutton, M.A., Cheng, M., Peters, W.H., Chao, Y.J., and McNeil, S.R., "Application of an optimized digital image correlation method to planar deformation analysis," *Image Vision Computing*, 4 (3), 143-150 (1986).

Vendroux, G. and Knauss, W.G., "Submicron deformation field measurements: part 2. improved digital image correlation," *Experimental Mechanics*, 38, 86-91 (1998).

Vendroux, G., "Correlation: A Digital Image Correlation program for displacement and displacement gradient measurements," GALCIT Report SM90-19, California Institute of Technology, (1990).

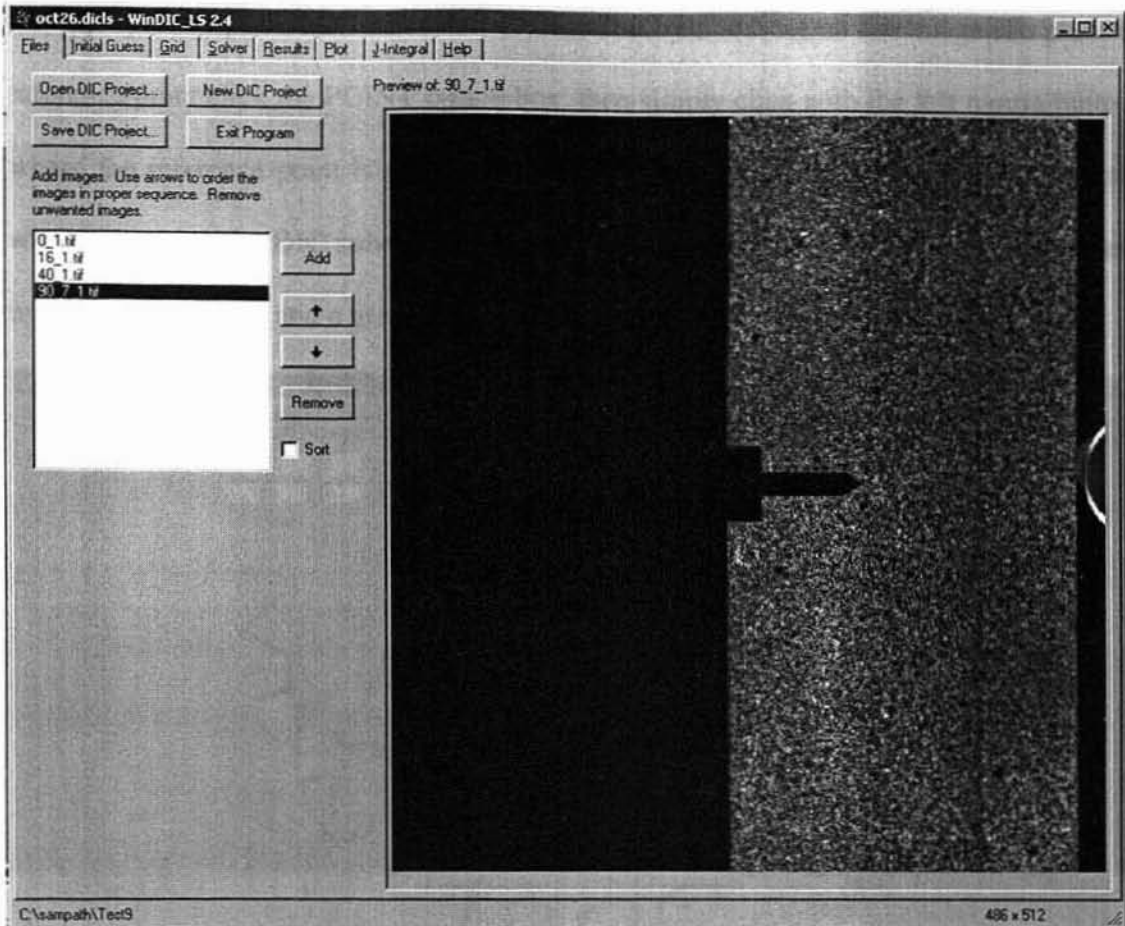
APPENDIXES

APPENDIX A

WINDIC_LS USER'S GUIDE

The WinDIC_LS program was developed to provide an efficient, user-friendly means if using the large deformation refinements to the digital image correlation method. There are eight basic modes of the program. The tabbed option box allows immediate access to the each of the five modes. Note that the origin (0,0) of the images is located at the lower left corner following the standard Cartesian coordinate system. Most other image manipulation programs set the origin at the left corner.

The FILES menu mode allows the user to Open the existing projects, save the current projects, start a new project and exit the WinDIC_LS program. Also in this mode, the user can add image files to be used in the digital image correlation. The list box shows the name of each of the images in the current project. The user must arrange the images in the order in which they will be correlated using the up and down buttons. Only 8-bit (256 level) grayscale uncompressed TIFF images are recognized with the current version of WinDIC_LS. If you want to use files that are stored in another file format, you must use a paint program Paint Shop Pro or some other software to convert the images in to the proper file format. Once the images have been selected then the user can proceed to the initial guess mode.



Mode 1: FILE MENU MODE

In most of the modes the toolbar is present for manipulating the displayed images. There are three zoom levels, Full scale, Zoom to fit the image the windows and Triple zoom. Also the arrows provide a way to switch between all the sets of images. At any time, the images can be panned around by holding down the right mouse button in one of the image windows and dragging the mouse around.

The initial guess mode is where the user will establish the initial guesses the DIC solver will use when starting the correlation process. These initial guesses are calculated by the program from reference marks the user, located on each image. The reference marks can be either a single point or a vector. Select which type to be used by selecting

the appropriate option box. Points are represented by a red dot on the image. To place a reference point click the POINT option box, then simply click with the left mouse button where the reference point is to be located. This red reference point should be close to where you want the DIC solver to begin correlating the images. Vectors are represented by a red location dot and a green direction point.



Mode 2: INITIAL GUESS MODE

To place a vector reference, click the VECTOR option box then press and hold down the left mouse to place the red location dot and then drag the mouse to locate the green direction dot and finally release the left mouse button.

In situations where the deformation does not have significant rotation, then the POINT type reference will allow the program to simply compute guesses for the initial offset parameters. All the other mapping parameters will be given an initial guess value of zero. In situations where the deformation has large rotation angles, the VECTOR reference type will allow the program to compute better initial guesses for both the location and first order gradients. The program will assume the higher order mapping terms are zero. After the reference marks have been positioned, the program will be ready to position the grid of nodes in the reference image.

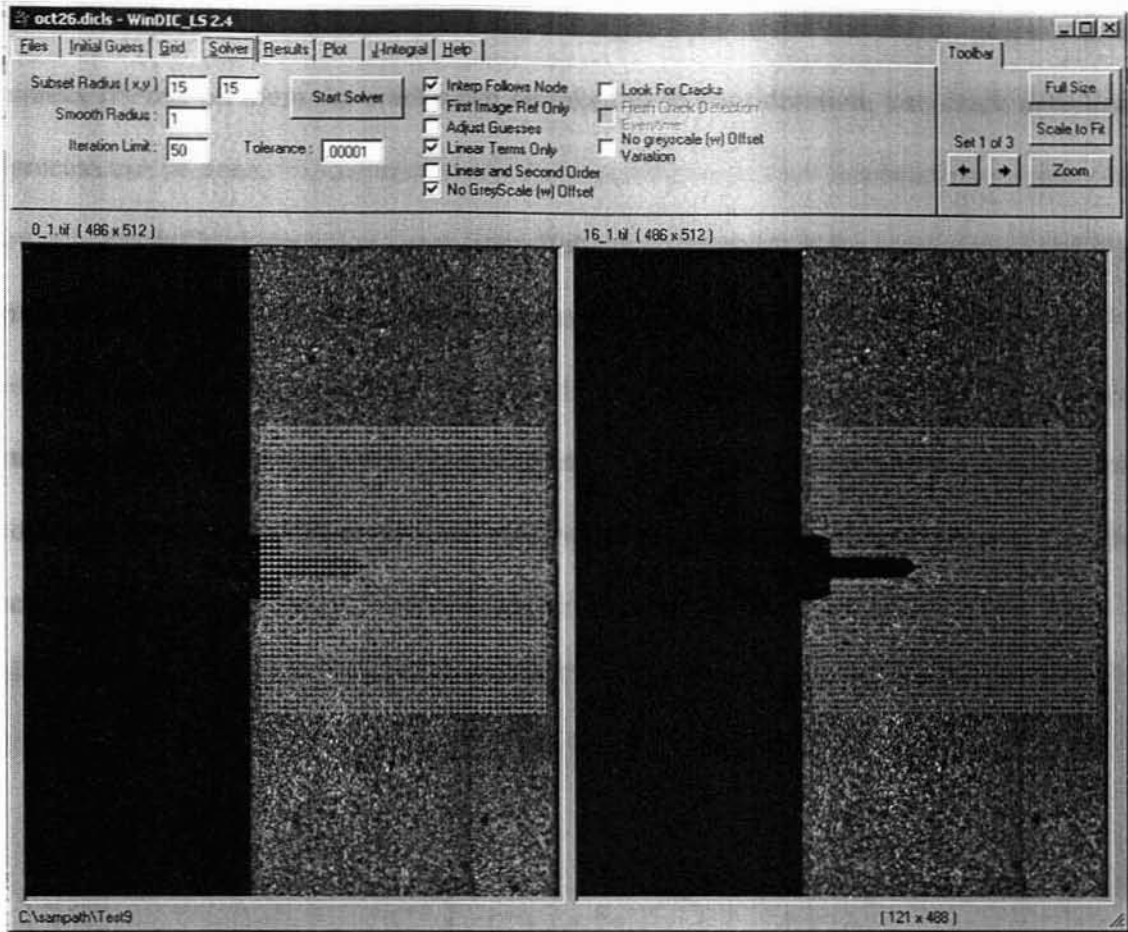


Mode 3: Grid Menu mode

The Grid Menu mode is where the grid of nodes is generated and located in the reference image. The first reference image is always displayed in the left image window. Use the mouse to locate the grid by pressing the left mouse button and dragging the grid to the desired position. The grid parameters can be modified by changing their values in the corresponding boxes. The grid will automatically change when the box that the grid parameter has been changed loses keyboard focus. The grid can be generated in several different patterns. The pattern determines the sequence in which the nodes are analyzed. In the grid mode you will notice a dashed magenta box around the grid of nodes and also in the right image window. This represents the approximate area of the images that will be used in the DIC procedure. The user will want to make sure that this region does not fall outside the boundary of the actual image it the solver will most likely generate an error.

The SOLVER menu mode provides the final set of solver settings. The SUBSET RADIUS sets the radius around a node that will be used to correlate the two images together. The smooth radius is used to smooth the image grayscale values. Using a value of zero will turn the image smoothing off. The iteration limit sets the maximum number of iterations each node will be allowed to converge on a solution. The tolerance is the maximum amount each of the mapping parameters can change before the solution is considered converged.

There are several option boxes so that different orders of displacement gradient terms can be calculated.



Mode 4: SOLVER MENU MODE

First order reference only: This option is used to make the computations with the first image as reference when there are more than two images. This makes the computation to be a cumulative one, so the displacement results are cumulative results.

Linear terms only: when this option is turned on the displacement calculations will be based on the first order terms only. The second and third order terms will not be computed.

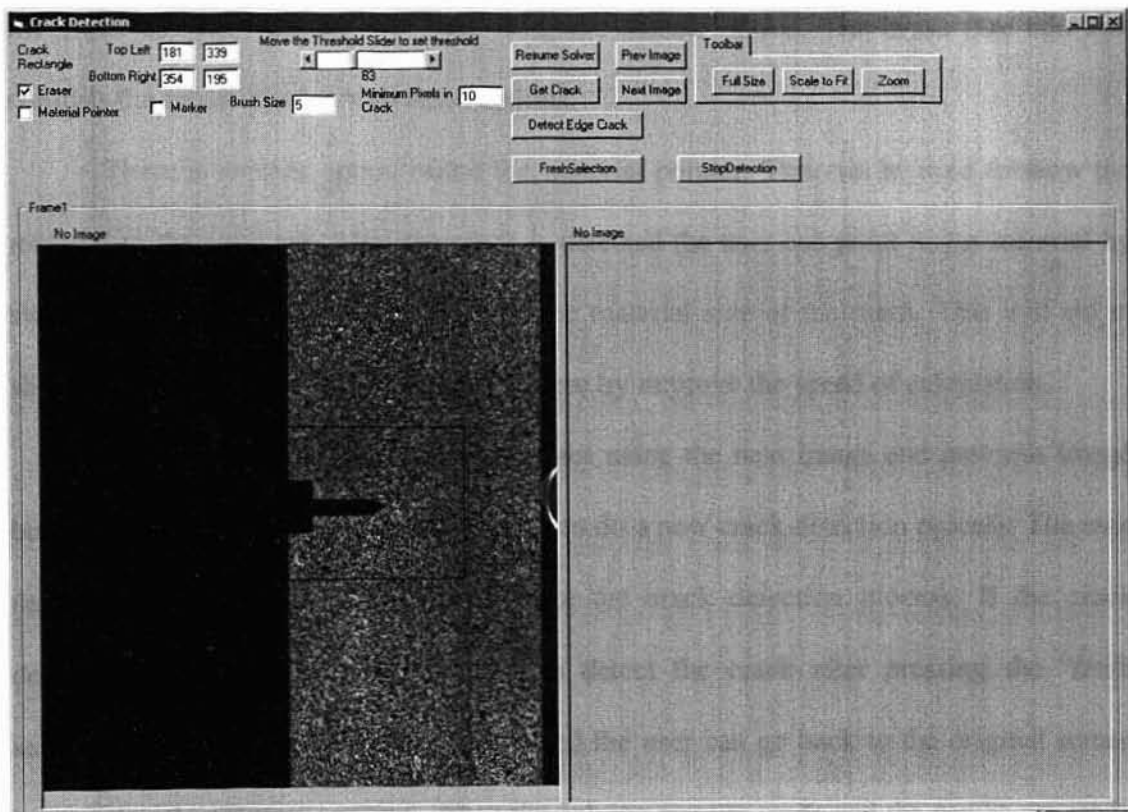
Linear and second order: When this option is turned on the displacement computations will be based on the first and the second order terms together.

No grayscale offset: The grayscale offset will not be taken in to consideration.

Look for cracks: When the images that are used in the correlation process have cracks present on them the cracks can be taken in to consideration, i.e., crack detection process can be done.

Fresh Crack detection every time: If the correlation stops for some reason and if it is to be started again without detecting cracks again, this option is to be turned on.

Crack detection menu mode is used to detect the crack on the specimen. When user clicks Start solver button on the solver menu mode the software enters in to the crack detection menu mode. Here the user can draw a rectangle around the crack to detect the crack.



Mode 5: CRACK DETECTION MENU MODE

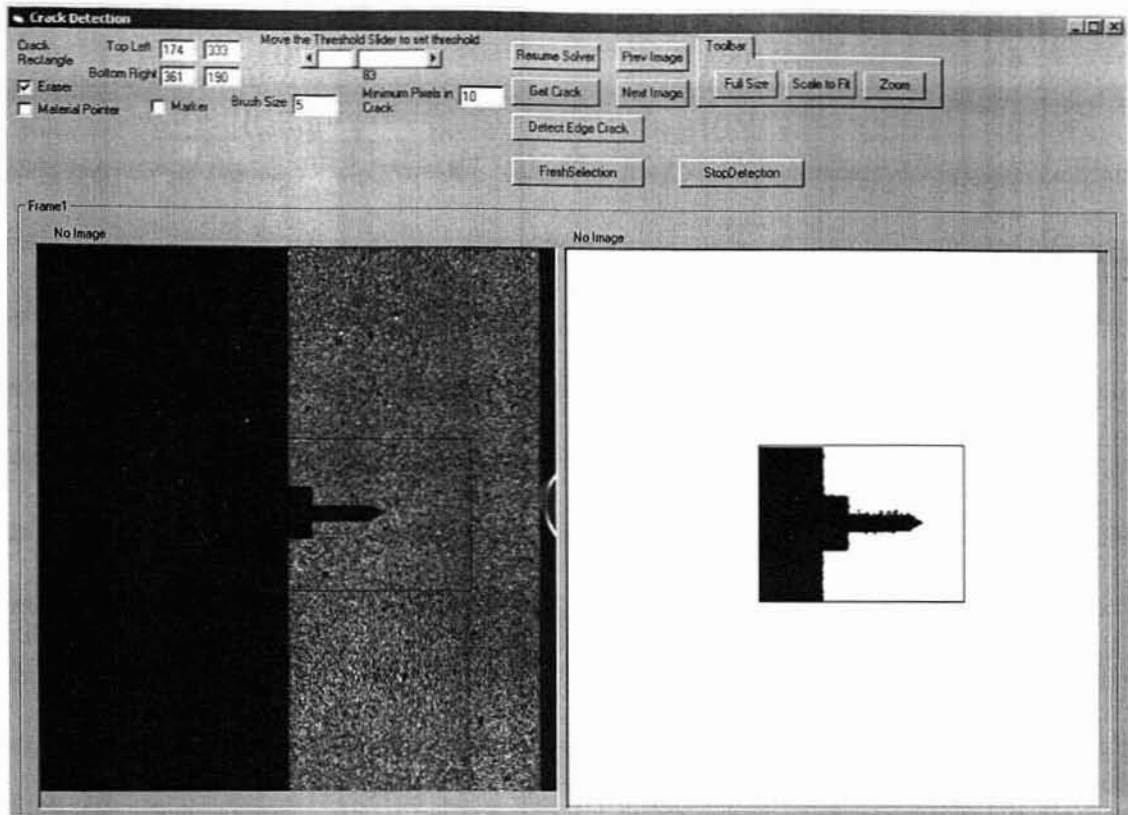
When the detect crack button is pressed the crack detection process starts, after this detect edge crack can be pressed (if the image used has edge crack in it). The crack

detected appears as black and white region on right hand side of the screen, as can be seen in the figure below.

The threshold value to be used during crack detection can be chosen using the slider bar present in this menu mode. The number of pixels in the crack can also be varied by using the edit box as can be seen on the figure. Editing of the crack detected can be done using some options present on this form. The size of the brush can be changed using the brush size edit box. The user can enter the desired value for the brush size. There are options for erasing and drawing on the screen. If there are unwanted parts on the crack detected they can be removed by using the eraser option. If some pixels are to be added to the crack detected that can be done using the marker option. The brush size edit box controls the brush size for both these options.

There is another option called the material pointer. This can be used to show the material to the software. After the crack is detected the user can point to the material by switching on this option and clicking on the material side of the crack. This will aid in showing the material to the software and there by improve the speed of calculation.

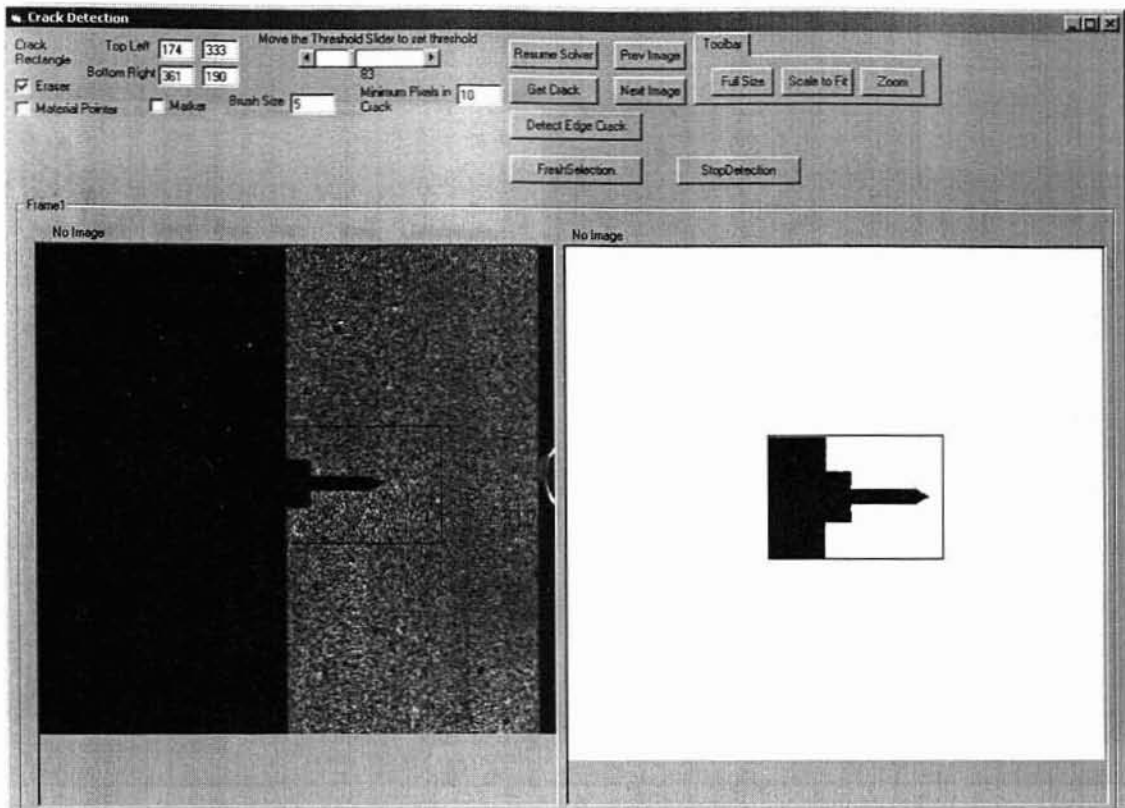
The user can traverse between images using the next image and previous image buttons. Fresh selection button can be used to do a new crack detection process. The stop detection button can be used to terminate the crack detection process. If the crack detection is not satisfactory the user can detect the crack after pressing the “fresh selection” button. After the crack is detected the user can go back to the original screen by pressing the “Resume solver”. Then the solving process starts and the results are ready for some time. The user can go to the results menu mode to view the displacement and deformation results.



Mode 6: CRACK DETECTION MENU MODE WITH THE DETECTED CRACK

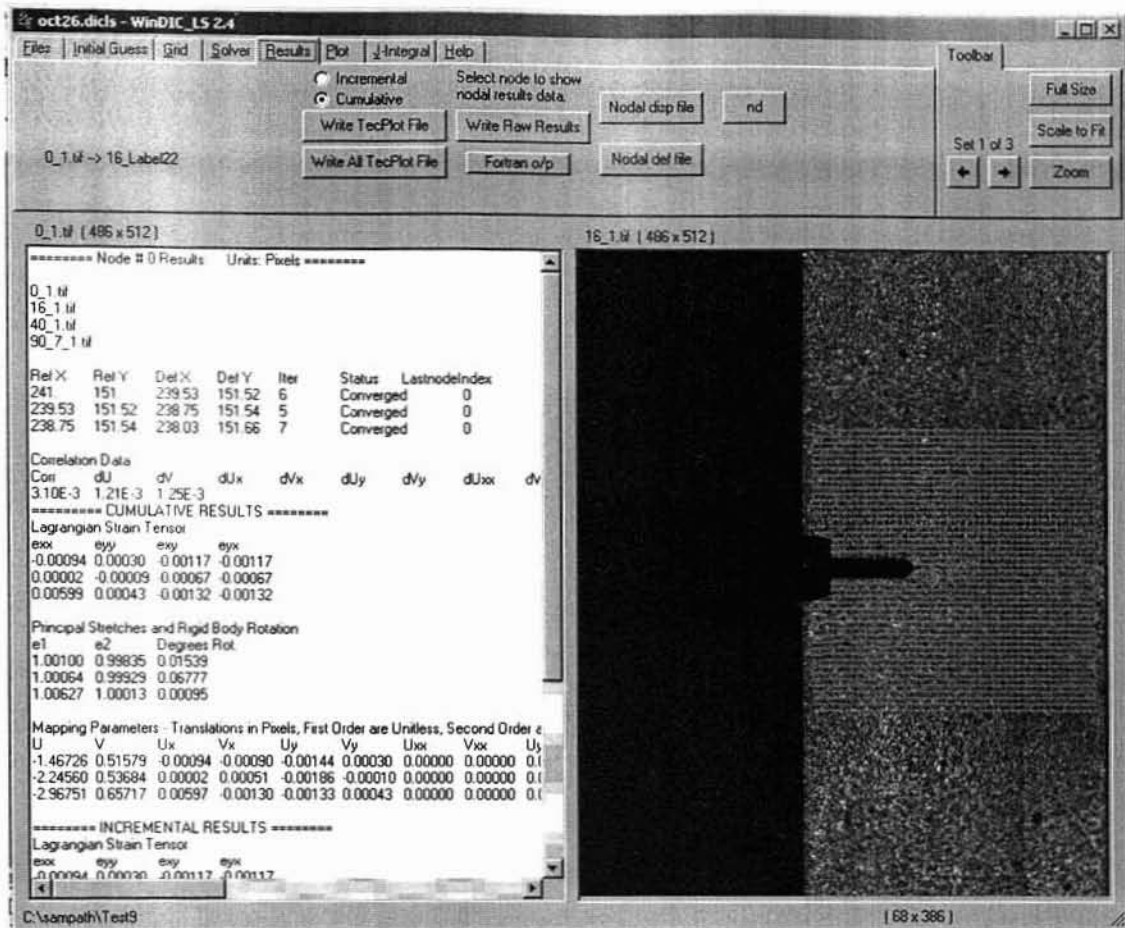
Important thing to be taken care of during the crack detection step is that the area selected should be small and closer to the crack, so that the crack detection will take place soon. As can be seen from Mode 6, the rectangle drawn surrounding the crack is close enough to the crack region. This allows the crack to be detected soon and the modifications if any can be done soon. The nodal grid placed on the reference image is not visible during this mode.

The results menu mode allows an easy way to look at the results of correlation. The left pane shows the complete set of results for a single node. To select another, simply select that node in the image display on the right and its results will be displayed in the information window.



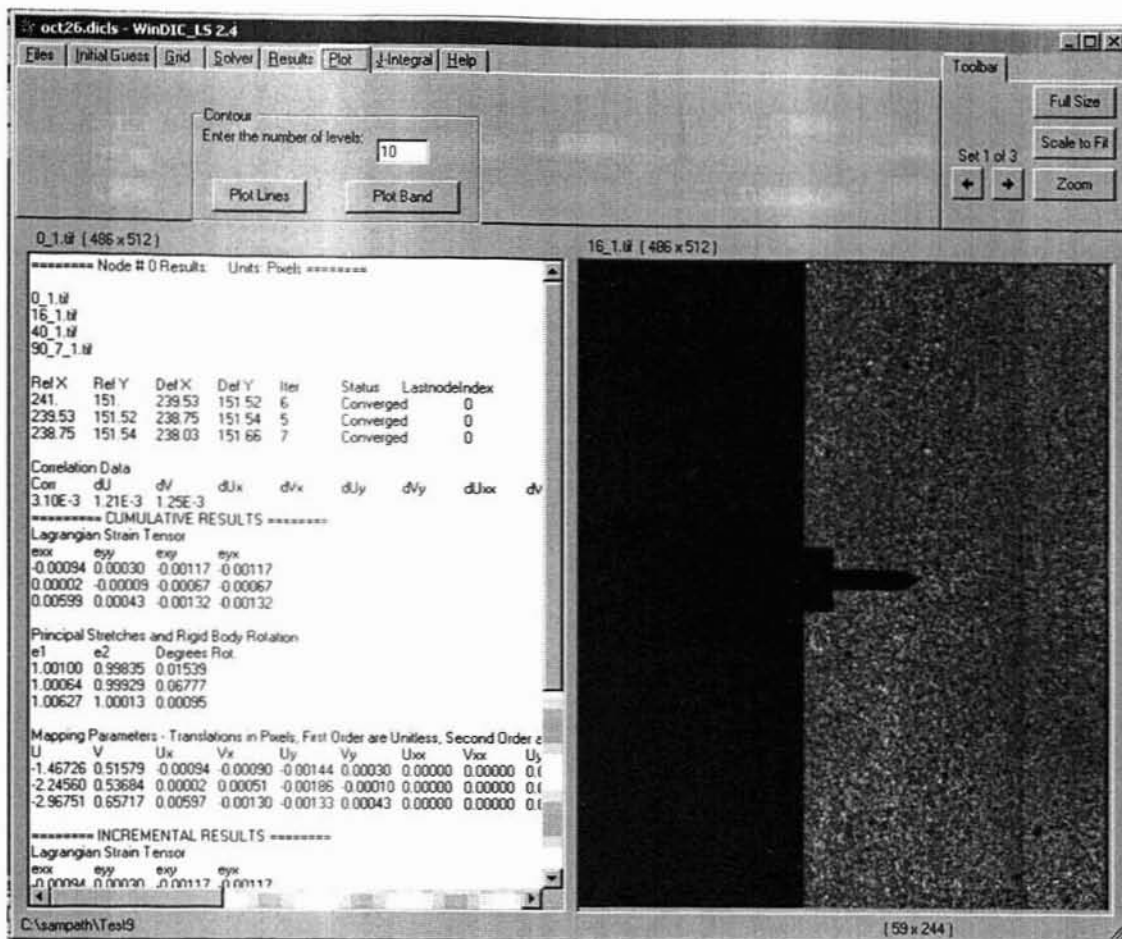
Mode 7(a): CRACK DETECTION MENU MODE WITH THE CRACK AFTER ERASING UNWANTED PARTS OF THE CRACK.

Mode 6(a) shows the crack after the unwanted parts of the crack have been removed using the eraser option in the crack detection screen. As can be seen from the figure, the crack alone is detected and taken. This helps in improving the algorithm by taking only the crack region in to account and not the part of the specimen. After the crack is detected the solver can be started to perform the computation of deformation for the specimen.

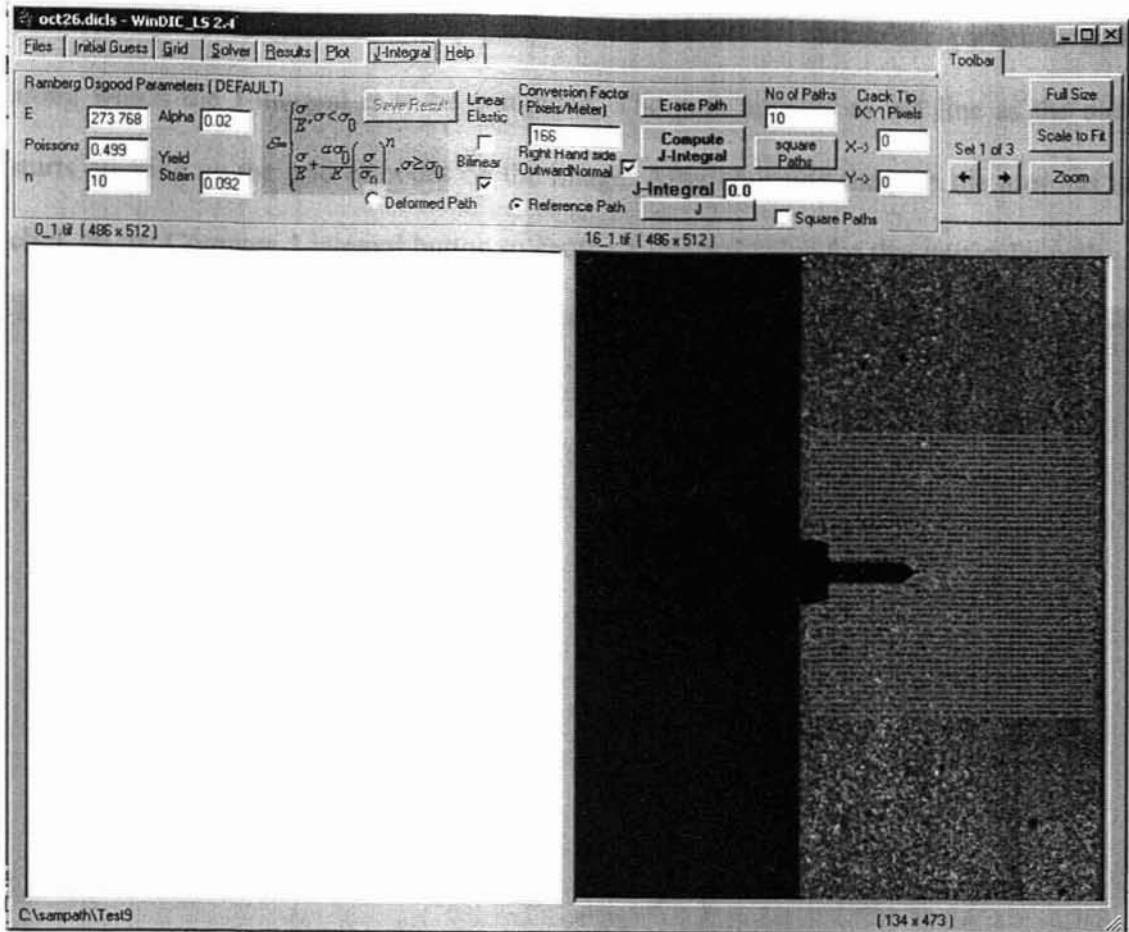


The program can also output a tecplot data file containing either the incremental or the cumulative results of the image shown in the image display. Incremental results are just the results of the deformation from the previous image. Cumulative results are the results from the first image to the selected image. The write raw function outputs a comma-separated list of all the data generated by the WinDIC_LS program. This raw file can be easily read into a spreadsheet program like Excel, or used as inputs to other programs.

In the results mode the user can generate files with various kinds of outputs namely nodal displacement file, nodal definition file and nodal files.



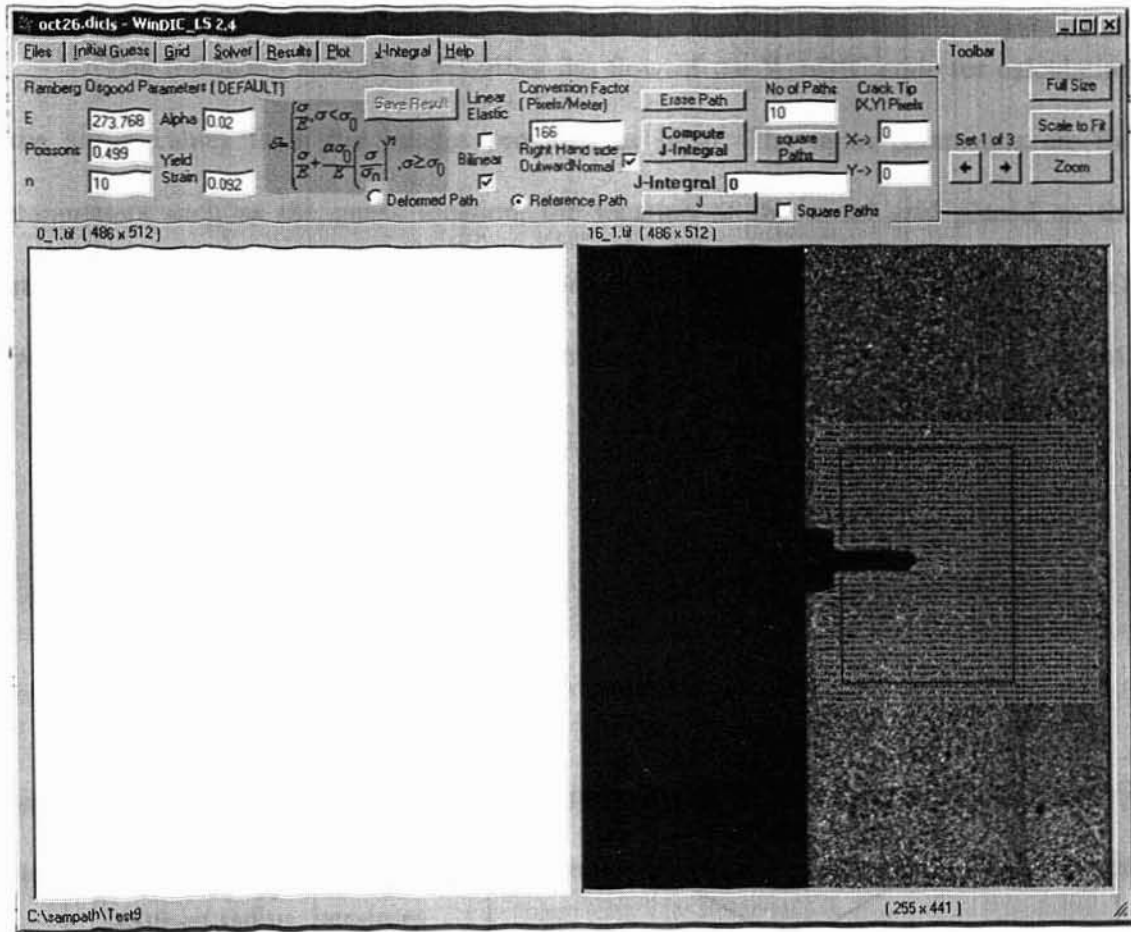
After the results are computed the strain values can be plotted on the images as bands or as lines in the plot menu mode. The user can choose the number of levels for the band and line plots. Based on the number of levels the plots will be made in the form of color lines or bands on the images. The plot lines and plot bands will appear to the extent of the nodal grid placed as the results are available only for that region of the specimen surface. When the plot is displayed on the image a scale will appear on the side to show the range of values in a scale. The user can traverse to different images with the buttons provided on the interface.



Mode 10: J-INTEGRAL MENU MODE

The J-integral menu mode allows the user to calculate the J-integral after the computation of the deformations for the nodes on the grid are over. There are provisions for entering the material properties such as Young's modulus (E), alpha, n the hardening coefficient and yield strain. The conversion factor should also be entered. It is the number of pixels per millimeter. The user has the option of choosing which the theory by which the stresses are to be calculated. The choices are linear elastic, bilinear as can be seen on the screen. If none of these two are chosen Ramberg-Osgood model will be chosen for calculating the stresses. When J-integral is computed for square paths then the crack tip location that is in terms of pixels should be entered.

After entering the necessary parameters the user can choose the particular path along which the J-integral is to be computed. The path appears as red line as the user starts clicking on the grid of nodes on the image. After choosing the path the user has to click on the Compute J-integral button to get the J-integral value for that particular path.



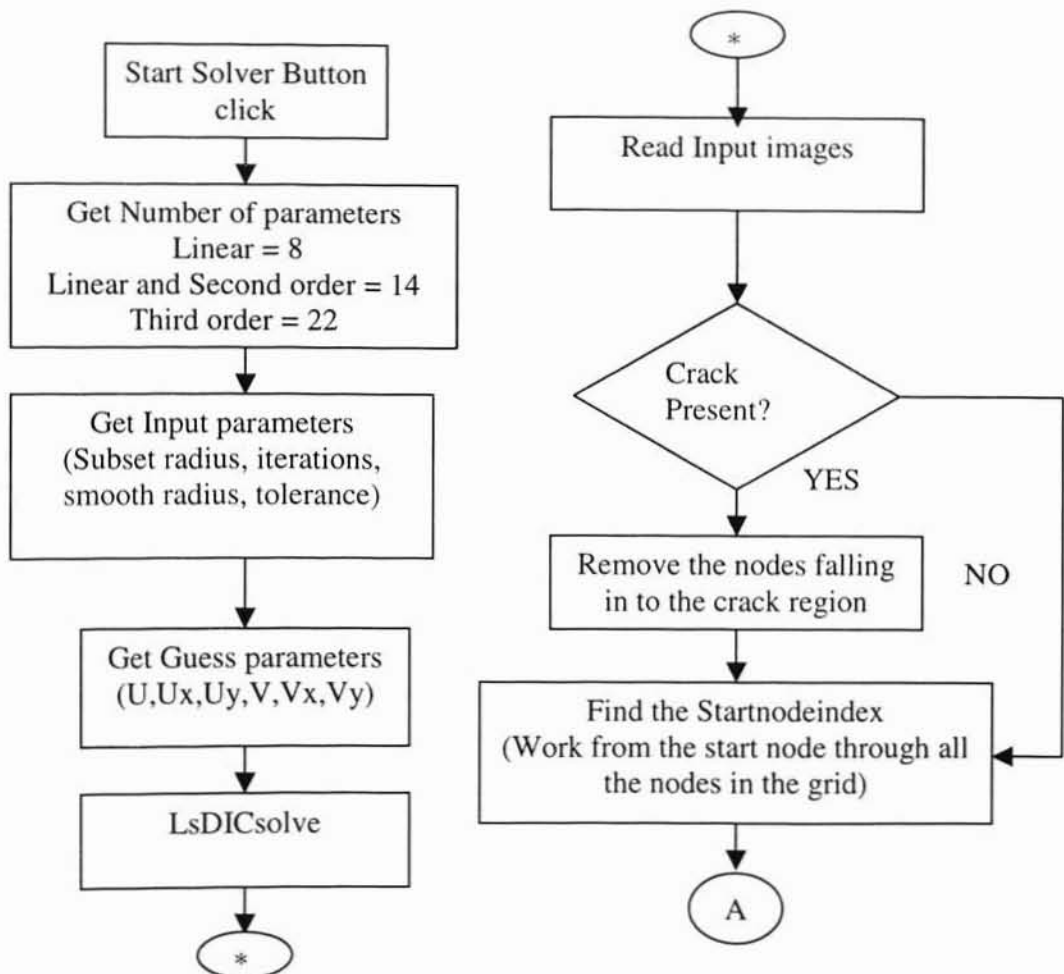
Mode 11: J-INTEGRAL MENU WITH PATH CHOSEN

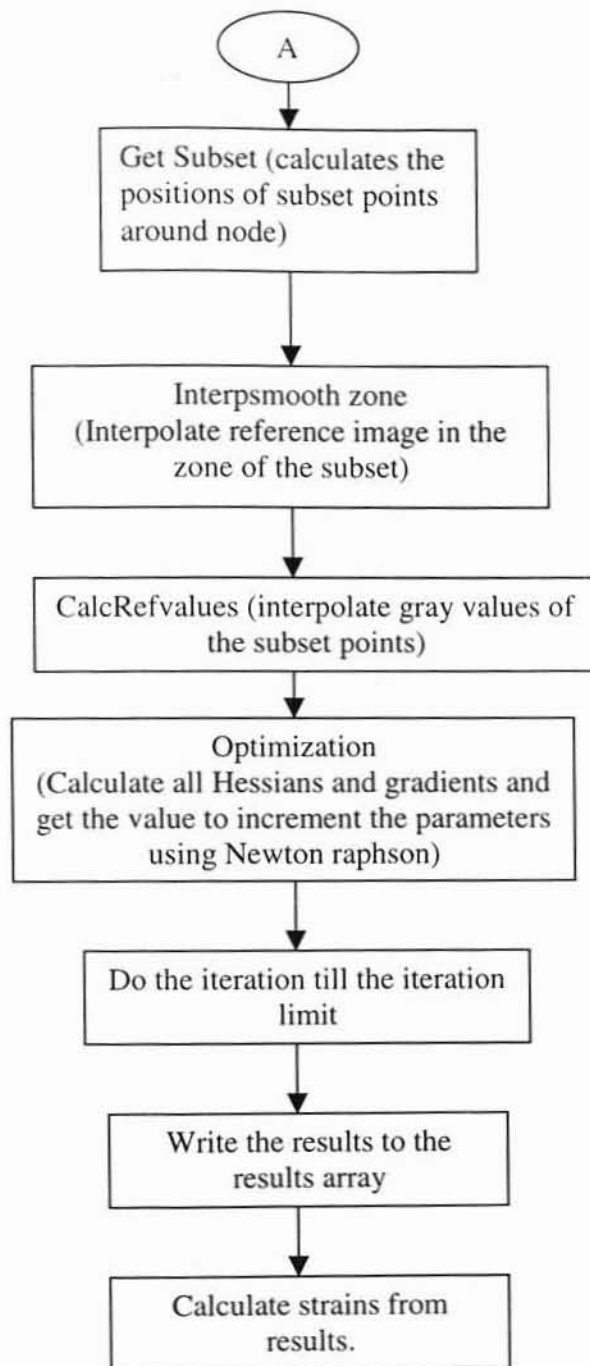
This program has been completely developed using Microsoft Visual Basic 6.0.

APPENDIX B

FLOW OF CODE FOR WINDIC

The following flowchart describes the flow of the WinDIC code for calculating the strain values from the images provided as input. The input parameters are the parameters such as the guess location, the location of the nodal grid placed on the reference image. Basic assumption is that the images are related to one another, in such a way that the grayscale pattern from the reference image to the deformed image is present.

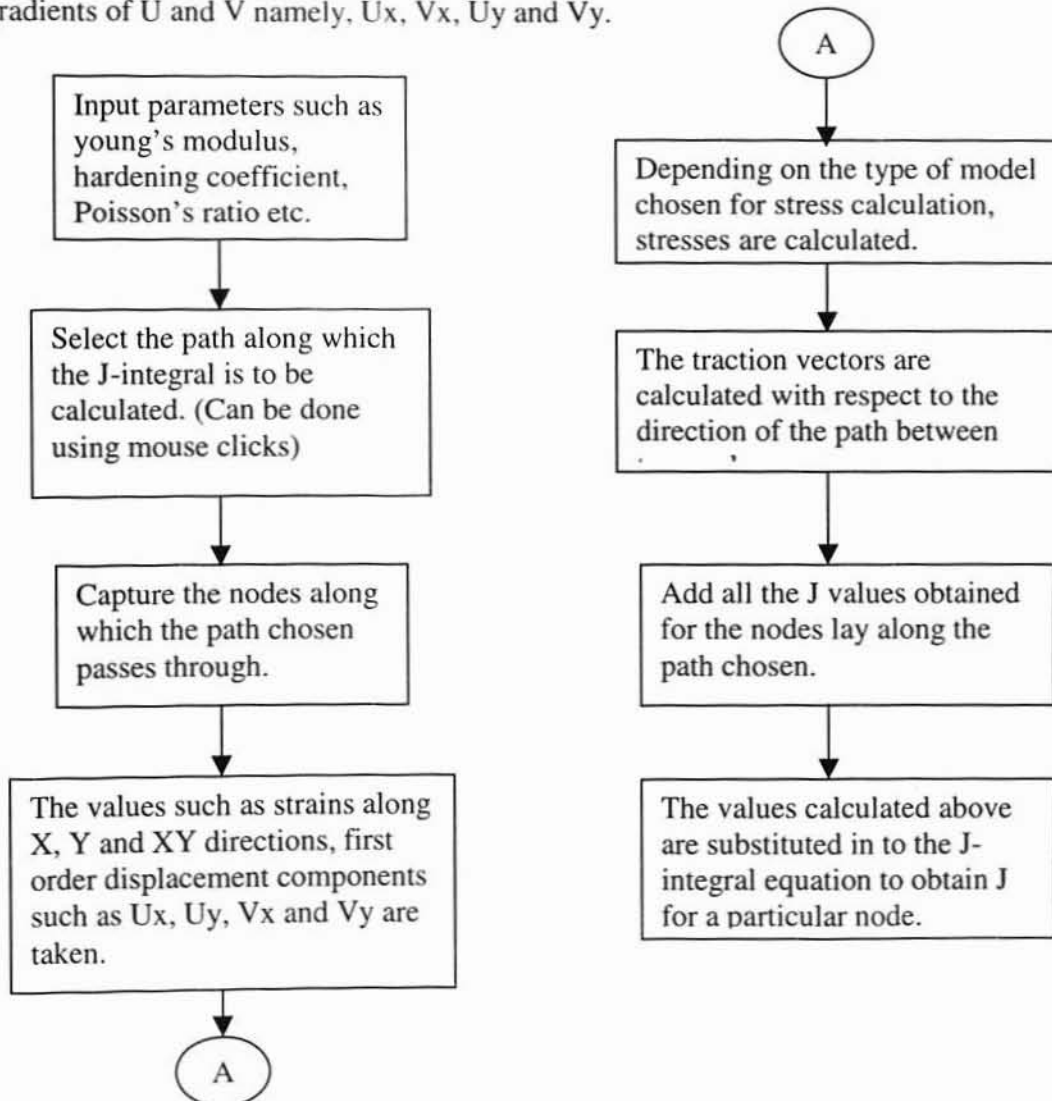




APPENDIX C

FLOW OF CODE FOR J-INTEGRAL COMPUTATION

The following flowchart describes the flow of code for the J-integral computation. The input parameters for the J computation are the data of the nodes that are on the path chosen along which J is needed to be calculated. The input parameters are first order gradients of U and V namely, U_x , V_x , U_y and V_y .



APPENDIX D

DEFORMED IMAGEMAKER USER'S GUIDE

The DeformedImageMaker is a Visual Basic program used to generate a reference image from the given deformed image. It is used in developing ideal images, which can be used for validation purposes. The user can get a reference image from a given deformed image. The figure below shows the user interface of the program.

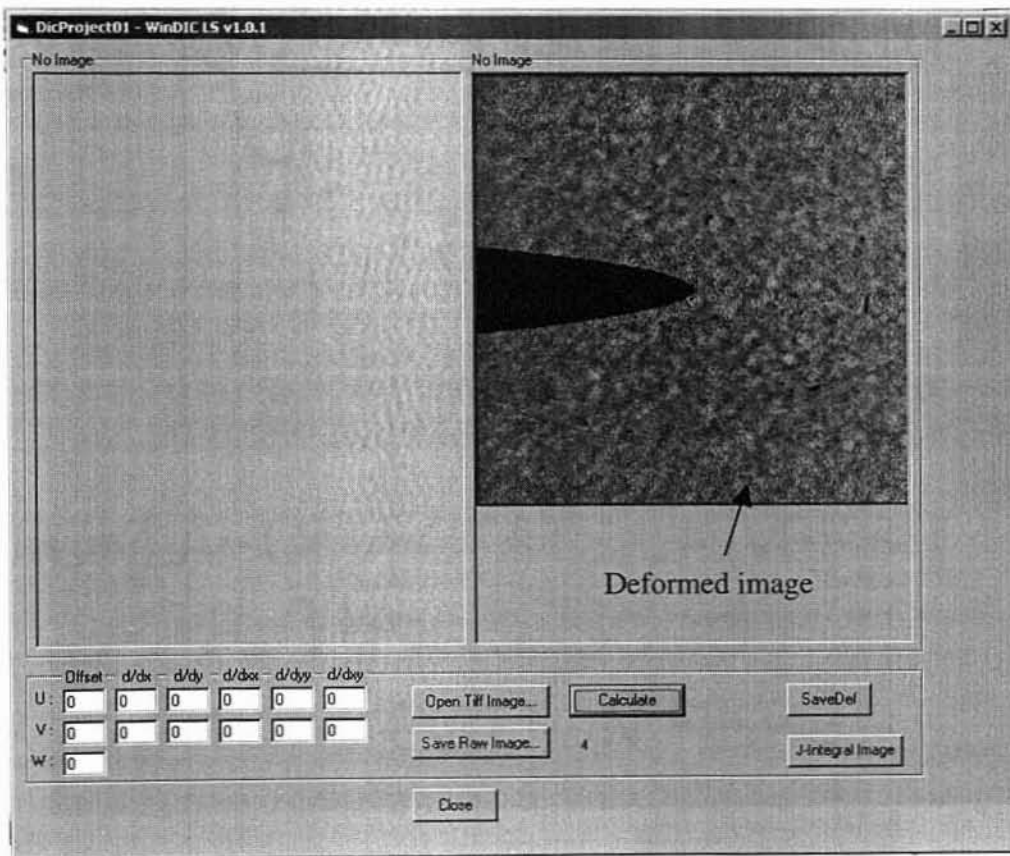


Figure 1 : User Interface of Deformed ImageMaker program with deformed image

The "Open Tiff Image" button can be used to get the deformed image as input in to the program. The user can input the parameters such as U, V and the first order and second order gradients in to the software to get the corresponding reference image. The calculate button is used to start the program to get the reference image from the deformed image.

After the calculations are over the reference image gets displayed in the left hand side as shown in Figure 2. The reference image can be saved using the "Save Raw Image" button. The raw image can be converted to TIFF format to be later used in WinDIC program. Thus the DeformedImageMaker can be used to get a reference image from a given deformed image.

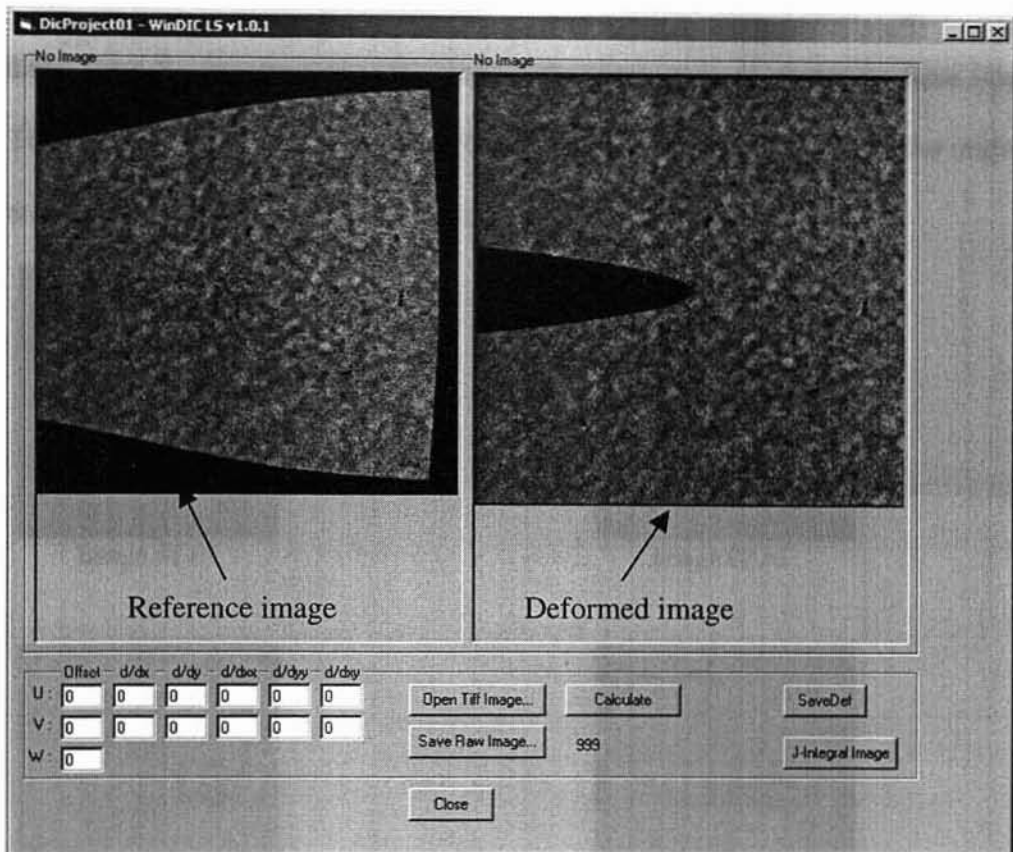


Figure 2: After calculation.

APPENDIX E

IMAGES USED IN THE UNIAXIAL TENSILE TEST ON PARTICULATE COMPOSITES

Following are the images that were used in the uniaxial tension test on particulate composites. The images show that the specimen has natural texture on its surface, which shows that there is sufficient grayscale pattern required for conducting Digital image correlation. From the images it can be seen that the crack starts to propagate from image 05.tif. The variation of J-integral values obtained can vary at about 20% from the original value because of the inhomogeneity in the particulate composite material.



Image 01.tif



Image 02.tif

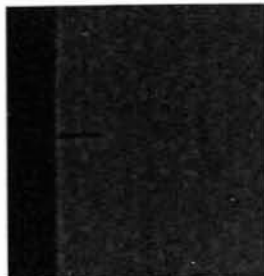


Image 03.tif



Image 04.tif



Image 05.tif



Image 06.tif



Image 07.tif

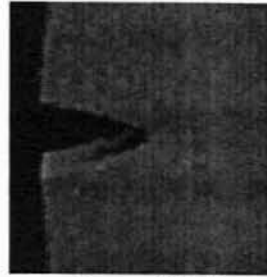


Image 08.tif

APPENDIX F

IMAGES OF PARTICULATE COMPOSITE USED IN 20% PRE-STRAIN TEST

Following are the images that were used in the uniaxial tension test on particulate composites. The images show that the specimen has natural texture on its surface, which shows that there is sufficient grayscale pattern required for conducting Digital image correlation. From the images it can be seen that the crack starts to propagate from image 12.tif.



Image 01.tif



Image 10.tif



Image 11.tif



Image 12.tif



Image 13.tif



Image 14.tif

APPENDIX G

IMAGES OF PARTICULATE COMPOSITE USED IN 15% PRE-STRAIN TEST

Following are the images that were used in the uniaxial tension test on particulate composites with 15% pre-strain. The crack propagation is from Image 12.tif to 14.tif.



Image 08.tif



Image 12.tif



Image 14.tif



Image 15.tif



Image 18.tif

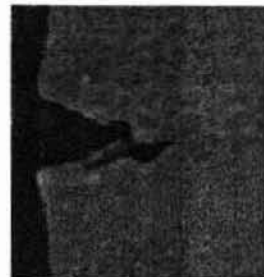


Image 19.tif

VITA 2

Sampathkumar Periasamy

Candidate for the Degree of

Master of Science

Thesis: DIGITAL IMAGE CORRELATION FOR DEFORMATION
MEASUREMENTS NEAR A CRACK

Major Field: Mechanical Engineering

Biographical:

Education: Received Bachelor of Engineering in Mechanical engineering from Government College of Technology, Coimbatore, India in June 1999. Completed the requirements for the Master of Science degree with a major in Mechanical Engineering at Oklahoma State University in December 2002.

Experience: Employed by Oklahoma State University as graduate research assistant, from October 2000 to July 2002 and subsequently as graduate teaching assistant, from August 2002 to December 2002.

Professional Memberships: American Society of Mechanical Engineers.